fractal and fractional

MDPI

Article

Uncertainty-Based Scale Identification and Process–Topography Interaction Analysis via Bootstrap: Application to Grit Blasting

François Berkmans [1,2,3], Julie Lemesle [4,5], Robin Guibert [1], Michal Wieczorowski [2], Christopher Brown [6] and Maxence Bigerelle [1,*]

[1] Univ. Polytechnique Hauts-de-France, CNRS, UMR 8201 - LAMIH - Laboratoire d'Automatique de Mécanique et d'Informatique Industrielles et Humaines, F-59313 Valenciennes, France; francois.berkmans@uphf.fr (F.B.)
[2] Institute of Mechanical Technology, Poznan University of Technology, Plac Marii Sklodowskiej-Curie 5, 60-965 Poznan, Poland; michal.wieczorowski@put.poznan.pl
[3] Univ. Polytechnique Hauts-de-France, INSA Hauts-de-France, LARSH - Laboratoire de Recherche Sociétés & Humanites, F-59313 Valenciennes, France
[4] Valutec, Univ. Polytechnique Hauts-de-France, 59314 Valenciennes CEDEX 9, France; julie.lemesle@uphf.fr
[5] U.R Concept, 59300 Valenciennes, France
[6] Surface Metrology Laboratory, Worcester Polytechnic Institute, Worcester, MA 01609, USA; brown@wpi.edu
* Correspondence: maxence.bigerelle@uphf.fr

Abstract: Finding the relevant scale to observe the influence of a process is one of the most important purposes of multiscale surface characterization. This study investigates various methods to determine a pertinent scale for evaluating the relationship between the relative area and grit blasting pressure. Several media types were tested alongside two different methods for calculating the relative area and three bootstrapping approaches for scale determination through regression. Comparison with the existing literature highlights innovations in roughness parameter characterization, particularly the advantages of relative area over traditional parameters like Sa. This study also discusses the relevance of different media types in influencing surface topography. Additionally, insights from a similar study on the multiscale Sdq parameter and blasting pressure correlation are integrated, emphasizing a scale relevance akin to our Sdr method's 120 µm cut-off length. Overall, our findings suggest a pertinent scale of 10,000 µm^2 for the Patchwork method and a 120 µm cut-off length for the Sdr method, derived from bootstrapping on residual regression across all media. At the relevant scale, every value of R^2 inferior to 0.83 is not significant with the threshold of 5% for the two methods of calculation of the relative area. This study enhances the understanding of how media types and blasting pressures impact surface topography, offering insights for refining material processing and surface treatment strategies.

Keywords: surface topography; multiscale analysis; grit blasting; fractal analysis

Academic Editor: Carlo Cattani

Received: 13 November 2024
Revised: 5 January 2025
Accepted: 13 January 2025
Published: 17 January 2025

Citation: Berkmans, F.; Lemesle, J.; Guibert, R.; Wieczorowski, M.; Brown, C.; Bigerelle, M. Uncertainty-Based Scale Identification and Process–Topography Interaction Analysis via Bootstrap: Application to Grit Blasting. *Fractal Fract.* **2025**, *9*, 48. https://doi.org/10.3390/fractalfract9010048

1. Introduction

1.1. Grit Blasting and Surface Metrology

One of the primary challenges of multiscale characterization studies is to model the relationship between a manufacturing process and its influence on surface topography [1,2]. These studies on the relationships between manufacturing techniques and surface condition aim at establishing a cause-and-effect relationship. Grit blasting stands out as a widely employed surface treatment technique, traditionally used for surface cleaning and rust elimination. In contemporary applications, it finds extensive use in altering surface roughness to achieve complex functionality. Grit blasting alters the surfaces of zirconium ceramics in

dental applications, where blasted surfaces enhance the biaxial strength and reliability by inducing compressive residual stresses [3]. One could also mention other applications such as improving cell adhesion [4] and increasing wettability or super hydrophobicity [5,6]. Grit blasting process variables affect blasted surface states. These process variable factors include grit blasting times, which influence the coverage, the nozzle orientation relative to the workpiece surface, the type of blasting material (including silica sand), as well as the workpiece material, and the blasting pressure.

Studies that investigate the relationship between the surface condition and the grit blasting process conduct the following:

- Examine the impact of changing a single factor in the process on roughness;
- Consider multiple factors and their interactions;
- Focus on surface analysis to select relevant characterization roughness parameters and observation scales;
- Concern the fractal dimensions of sandblasted surfaces.

Bouzid and Bouaouadja [7] argued that the maximum height of the profile (Rt) increases with the angle and blasting duration, while the Ra is found to only increase with blasting duration [8]. Regarding the size of the materials, several studies agree that roughness increases when the surface is blasted with finer materials. The study of Su et al. [9] compares powders of 50 μm and 110 μm on zirconia. The geometry of the blasting grit significantly affects the surface topography: smaller grit sizes result in more homogeneous surface textures and lower Sa and Ra values compared to larger grits. As expected, the Ra values of the surfaces of the TA6V alloy increase with higher blasting pressure for both 20/40 (300–850 μm)- and 180 (53–90 μm)-mesh garnet particles [10].

The study by Su et al. [11] presents the results of a comparison between all these factors on dental zirconia. The volume and height loss increased with higher grit blasting pressure and longer treatment duration but decreased with larger grit powder size. The Substrate Bonding Strength (SBS), which refers to the strength of adhesion between an applied layer and the underlying material, known as the substrate, significantly increased with longer grit blasting durations and larger alumina powder sizes. However, the SBS values did not differ significantly among different grit blasting pressures. The previous article does not express its results in terms of standards such as ISO 25178-2 [12] (roughness parameters), which are nonetheless crucial for the geometric characterization of surface topographies. On the other hand, the study by Valverde et al. [13] presents an investigation on a titanium alloy, providing the values of the roughness parameters as the results. Statistical analyses revealed that the Sa, Sq, and Sdr values were influenced significantly by the blasting media, velocity, and surface coverage (all $p < 0.001$). Moreover, the media velocity, the media coverage, and the interaction between the media and velocity, as well as the interaction between the media and coverage, significantly impacted the Sa, Sq, and Sdr values ($p < 0.002$).

Surface metrology focuses on characterizing surfaces using relevant parameters that best represent changes in geometry in a comparative study [14]. Previous studies merely discriminate between blasted surfaces using overly general parameters (e.g., Ra, Rt) to describe surface geometries. Relevant roughness parameters must also be analyzed at a pertinent scale which best isolates the features characteristic of the process, i.e., those influencing the surface topography. According to Ho et al. [15], the parameter that characterizes significant changes in morphologies in the grit blasting process is the Sdq from ISO 25178-2; Sdq describes a correlation between the blast pressure and surface roughness. Sdq represents the root-mean-square value of the surface slope within the sampling area. Sdq is computed using a Lagrangian polynomial with seven points in orthogonal directions [16,17]. The pertinent filtering scale for the Sdq parameter (i.e., the one that best

describes the change in topography induced by grit blasting) is a 120 µm low-pass filter in the study by Ho et al. [15] using 150–250 µm silicon carbide particles as the blasting medium for pressures from 1 to 7 bar.

1.2. Fractal Philosophy

Blasted surfaces are also studied using fractal dimension analysis, which is another method of multiscale characterization. Fractal structures and advanced material characterization are pivotal in enhancing the functional properties of materials and surfaces. Recent advances, such as the work of Yan et al. [18], have demonstrated the potential of engineered multilayer nanocomposites to overcome trade-offs between a high breakdown strength and the dielectric constant, achieving significant performance gains. This emphasis on multiscale strategies highlights the importance of advanced methodologies, including fractal-based approaches, in addressing challenges in surface and material characterization. Advanced material characterization plays a crucial role in bridging the gap between fundamental research and technological applications. For instance, O. Barros et al. [19] investigated the dielectric properties of $ZnNb_2O_6$ (ZNO) combined with $CaTiO_3$ (CTO), highlighting the impact of crystalline phase interactions on thermal stability and electromagnetic performance. Such studies underscore the importance of multiscale approaches and precise characterization techniques, which are also critical in understanding and optimizing surface properties across different domains.

Blasted surfaces exhibit self-affinity, meaning they have a structure that is similar at different scales. Persson's work [20] provides a kinetic model to understand how sandblasting generates a fractal surface, combining theoretical and experimental aspects. Blasting operates on the principle of transferring the kinetic energy of high-velocity particles to a target surface. Upon impact, the particles' energy is dissipated through multiple mechanisms, including plastic deformation, elastic rebound, and minor losses (e.g., noise and vibrations). Hutchings [21] suggested that 80% of the energy is converted into heat for metals, but the experimental work by Gillstrom and Jarl [22] estimated this fraction to be closer to 39% for steels, challenging prior assumptions. The energy balance during impact shows that only the energy associated with plastic work in the workpiece contributes to heat generation. Elastic energy causes rebound, which can be quantified using the coefficient of restitution. The rebound effect depends on the material properties, such as the hardness and elastic modulus. As shown in prior studies, softer materials absorb less energy as heat due to their higher hardness-to-modulus ratio, which enhances elastic recovery. The contact mechanics are described using the Hertz contact theory, as discussed by Timoshenko [23] for elastic contact time and Chaudri and Walley [24] for plastic contact time. The contact radius and time depend on the particle's velocity, size, and material properties. Maeda et al. [25] assumed the contact area to be the particle's projected area. However, numerous shot-peening and sandblasting experiments have demonstrated that the penetration depth during impact is significantly smaller than the particle radius. Studies on materials highlighting the effect of heat on titanium alloys indicate that the morphology can become unstable when exposed to a constant temperature of 400 °C for a certain period [26]. The localized heat generated by the impact of sandblasting is insufficient to cause such changes, particularly during a brief blasting of a few seconds like in our study [27].

In general, blasted surfaces are extensively studied for their fractal complexity because the grit blasting conditions vary the complexities of the surface topography [28–30].

This study builds on the study of Berkmans et al. [31] in which two methods of fractal-based characterization calculation were compared to determine the relative area with respect to scale. In summary, the Richardson Patchwork method, from the ASME B46.1 [32],

was compared with the Sdr parameter derived from ISO 25178-2 (Equation (1)) [12], using a low-pass Gaussian filter for multiscale characterization. Filtering methods are widely used in roughness analysis, providing a reliable and simple way to process 2D or 3D signals depending on how the surface profile is studied. Common methods include Gaussian [33–35], robust [36,37], and spline filters. Gaussian filters, standardized under ISO 16610-21 [38], are the most commonly used method [39].

$$Sdr = \frac{1}{A}\left[\iint_A \left(\sqrt{\left[1+\left(\frac{\partial z(x,y)}{\partial x}\right)^2+\left(\frac{\partial z(x,y)}{\partial y}\right)^2\right]}-1\right)dxdy\right] \quad (1)$$

The comparison is based on the relative area calculated from topographies of TA6V samples that were grit-blasted with different pressures and blasting materials (media). The surfaces produced by grit blasting exhibit fractal-like characteristics over the scales studied, allowing for the analysis of area development at multiple levels based on pressure and media. Both methods yield similar relative area results across a wide range of scales for a given blasting condition. The Patchwork method is clearly sensitive to complexities and to differences in pressure. The Sdr method, with our proposed protocol, is easier to implement with some conventional roughness software. This could make Sdr more practical for some analyses. The results of this study present the calculations of the relative area at different computation scales. Increasing the blasting pressure causes a work-hardening phenomenon on the surface, making it less rough at high pressures (8 bar) compared to intermediate pressures (5 bar) when using media such as glass beads. This results in a smaller relative area at 8 bar compared to 5 bar at the smaller scales for both methods (Figure 1).

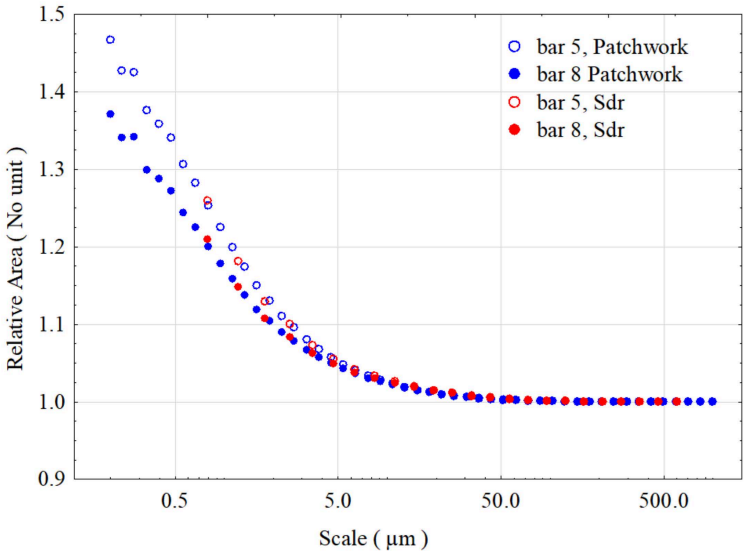

Figure 1. Comparison of two methods, Sdr (ISO 25178-2) and Patchwork, for calculating relative areas of surface topographies created by blasting with glass beads. The points represent the median of the relative area values, categorized by calculation method and pressure. Blue symbols indicate the median points for the Patchwork method, while red symbols correspond to the Sdr method. The scale refers to the cut-off length of the low-pass Gaussian filter applied in the Sdr calculation. For the Patchwork method, the tile size in μm^2 is equal to half the square of the cut-off length.

It should be noted that the equation of the Sdr parameter (Equation (1)) is inconsistent with fractal theory, as a fractal curve is non-differentiable.

The objective of this work is to propose a method to calculate the scale in the calculation of the relative area pertinent to the pressure of grit blasting. Based on the previous results, this method will contribute to improving the precision and reliability of surface area calculations, leading to more effective control and optimization of blasting processes in various applications. The method would allow for better characterization of the grit blasting process, as well as other manufacturing processes that create fractal surfaces with modifiable intensities, such as electrical discharge machining [40] and laser manufacturing [41].

2. Materials and Methods

2.1. Creation of the Blasted TA6V Surfaces

The data used in this publication come from the study by Berkmans et al. [31]. To control surface topography and avoid bias in subsequent statistical analyses, this study utilized grit-blasted TA6Vsurfaces. The workpiece cylinders, measuring 30 mm in diameter and 20 mm in height, were ground with SiC papers ranging from grit 80 to 4000 before grit blasting.

The TA6V surfaces were grit-blasted using the Guyson Euroblast 6SF system (Guyson S.A, Skipton, North Yorkshire, UK). Three types of grit materials were used: two types of glass silico-soda–calcium microbeads (G 100 with particle size of 70–150 µm and G 250 with particle size of 150–250 µm) from ARENA (Marquette-lez-Lille, France) and an abrasive material named C 300 50/80 (particle size of 100–630 µm) from Semanaz (Bray-Saint-Aignan, France), composed of hard, sharp, abrasive crystals manufactured from molten glass mass with a composition of silicate, alumina, and iron oxide.

Seven blasting pressures, ranging from 2 to 8 bar, were applied for each grit material, resulting in a total of 35 blasted TA6V samples. The specimens were divided into sets, one set for C 300, one set for G 100, and three sets for G 250, to study the repeatability of the grit blasting process. In preliminary experiments, 1 bar was included, but challenges were encountered in achieving a consistent and uniform surface topography, leading its exclusion from the main study.

During grit blasting, the distance between the blasting gun and the workpiece surfaces was maintained at approximately 10 cm. The grit materials were blasted perpendicularly to the TA6V surface for about 30 s for pressures ranging from 2 to 8 bar, ensuring a homogeneous blast across the entire surface. The blasting was performed with a back-and-forth motion (left to right) from the top to the bottom of the surface. This method provided a wide variation in the relative surface areas.

2.2. Topographical Measurements of the Blasted Surfaces

White-light interferometry (Bruker ContourGT™, San Jose, CA, USA) was used to measure the blasted surface topographies (Figure 2). Fifty 1×1 mm^2 regions, corresponding to stitching maps of 5059×5058 pixels (540 elementary maps), were measured randomly on each surface with a $50\times$ lens (elementary map size of 127×94.9 µm for a 0.198 µm X/Y resolution). A total of 1750 measurements were obtained from the 35 surfaces. Post processing, filtering and fractal calculations were performed on the dataset of the 1750 measurements (50 zones $\times$ 35 blasted surfaces) using the software MountainsMap 8® (Digital Surf, Besançon, France).

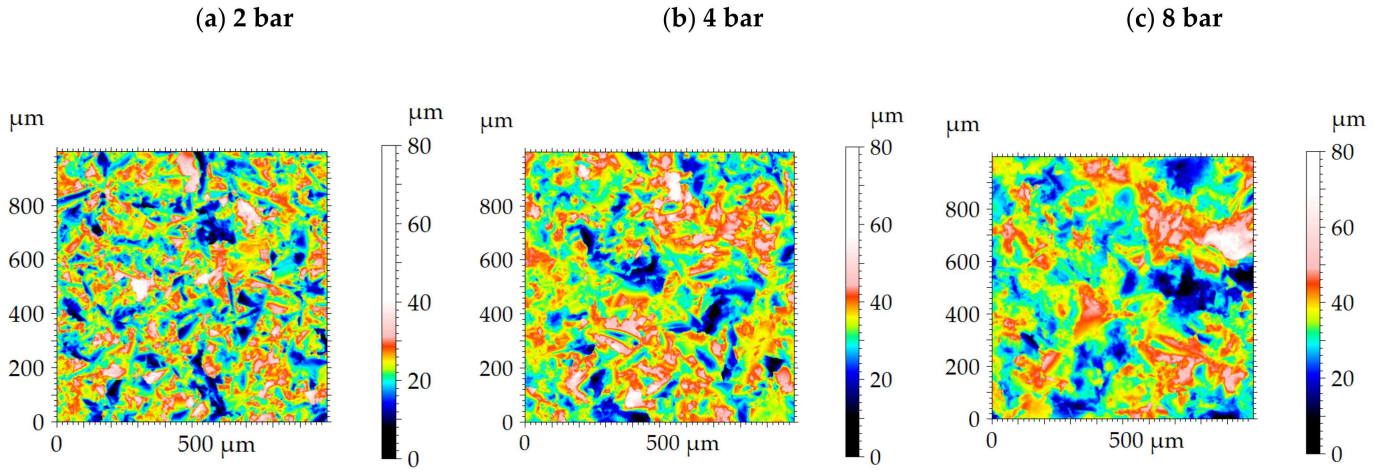

Figure 2. Surface topographies of TA6V surfaces grit-blasted at 2 bar (**a**), 4 bar (**b**), and 8 bar (**c**) with the C300 medium. The aggressiveness of the medium can make it difficult to assess visually the gradation in blasting intensity. More surface topographies are shown in Appendix A.

2.3. Methods of Relative Area Calculation

The methods used to calculate the relative surface area are fractal methods known as area-scale analyses. The first method is called the Patchwork method, developed by Brown in the 1990s [42]. The second is a method derived from the Sdr parameter of the ISO 25178-2 standard, with the addition of a low-pass Gaussian filter for the multiscale approach [31]. Brown's Patchwork method and the Sdr (Surface Area Ratio) method are both used to analyze surface roughness and topography, but they differ in how they define and calculate relative area. In the Patchwork method, the surface is divided into small triangular patches of constant size (Figure 3). These patches are created through interpolation between the regularly spaced measured heights on the surface. As a result, each triangular patch has a fixed, uniform area across the entire surface, regardless of the spacing or density of the measurement points. This constancy in patch size enables a local analysis of surface roughness or texture. The strength of this method lies in its ability to capture local variations in texture and provide a fine-grained statistical view of the surface irregularities. It is particularly useful for studies requiring multiscale characterization or the analysis of complex functional surfaces. On the other hand, in the Sdr method, the patches are not of constant size. They are defined by the sampling intervals on the surface, and their area varies depending on the height differences between these points. The Sdr measures the ratio between the real surface area of a topography, accounting for its features, and the projected surface (Figure 3). Thus, unlike the Patchwork method, the patch area in the Sdr calculation is variable and directly reflects the surface topographical complexity. The more pronounced the irregularities between the sampled points, the larger the patch area becomes, leading to a higher Sdr value. The Sdr is expressed as a percentage and is used to quantify the relative roughness of a surface compared to a flat reference surface. The key difference between these two methods lies in the areas of the triangular patches. In the Patchwork method, the area is constant, ensuring uniform and regular analysis, even if the vertices of the triangular patches are spread unevenly. In the Sdr method, the patch area is variable, influenced directly by the distribution of sampled heights and local asperities, providing an equally accurate representation of a measured surface. Formally, the Patchwork method is more closely related to fractal theory, as introduced by Benoît Mandelbrot in his study of the coastline of Great Britain, based on Richardson's data [43]. The fractal nature of the method lies in its ability to handle different scales, making it particularly suited to analyzing surfaces with varying roughness.

However, the Patchwork method has certain challenges. One difficulty can be the potential distortion of the patch shapes, which could lead to the Schwartz area paradox, if this is not controlled for. Correcting this deformation is straightforward, and the algorithms needed to address this issue are computationally simple. The Sdr method is easier to implement computationally, as it directly computes the ratio based on the sampled heights, without concerns about patch deformation; however, it depends on the filtering algorithm, which distorts the measured topography. Despite these differences, we can expect convergence between the two methods when dealing with surfaces that are not too rough, i.e., complex, at the scales being investigated. The distinction between these two calculation methods is presented in 2D form in Figure 3.

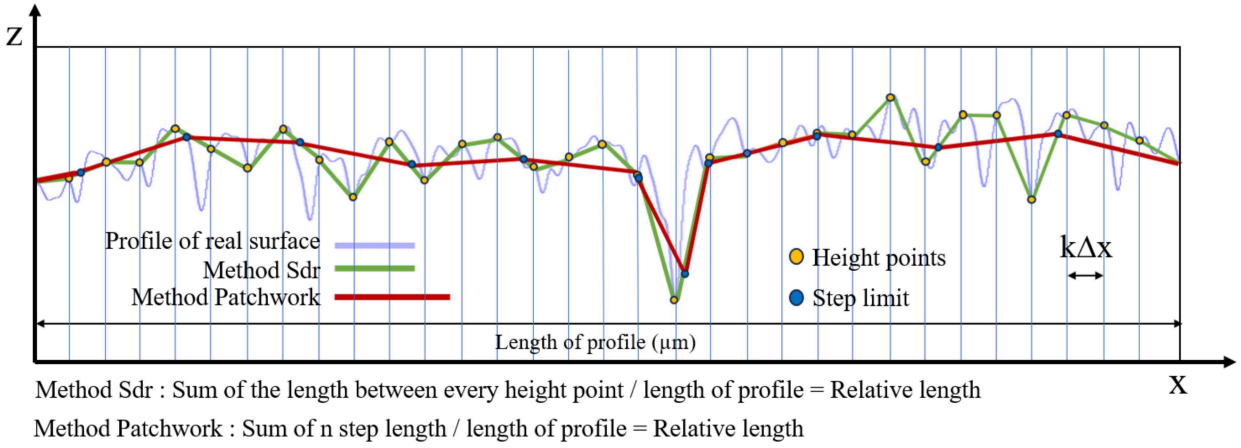

Figure 3. Diagram of the two calculation methods used in this study, shown in terms of relative length. The blue continuous line represents a real surface. The green line, a linear interpolation between measured height points, represents our measured profile (the Sdr method calculates the relative length at the sampling scale). The red line illustrates the profile obtained by the Patchwork method.

2.4. Statistical Analysis Based on Bootstrapping

2.4.1. Description of the Adopted Methodology

The results of linear regressions as a function of the scale used to calculate the relative area are used to evaluate the relevant scale for analyzing the relative area based on the pressure used; we present the results of linear regressions as a function of the scale used to calculate the relative area. The study presented here uses the principle of multiscale analysis for surface characterization. The principle is to examine the surface across multiple scale ranges and to associate findings or calculations with different scales [44]. In addition, a bootstrapping protocol is used to obtain robust results. Bootstrapping is a statistical method used to estimate the distribution of a sample statistic by repeatedly resampling with replacement from the original data. This technique helps assess the accuracy and variability of estimates, providing robust results even with small or non-normally distributed datasets [45]. The linear regressions in Figure 4 use replicated data (10 values of the relative area for each pressure are randomly selected out of the 1000 bootstrapped values) and were computed at the smallest scale of calculation for both methods. This provides us with initial information regarding the relevance of the scale. Indeed, for both calculation methods, the scale, where the relation of the relative area value depending on the pressure is high, is not the smallest scale that should be observed. The smallest reasonable tile size for the Patchwork method is one-half the square of the sampling interval (Figure 4a), while the cut-off length is 0.789 µm for the filtering used for the Sdr method (Figure 4b). Here, with very low determination coefficients R^2 (0.04 for the Patchwork method and 0.05 for Sdr), one can consider that analyzing the surface in maximum detail does not show the influence

of pressure on the relative area. This could be due to the work-hardening phenomenon and media size [46], which flattens the surface and makes it less complex as pressure increases.

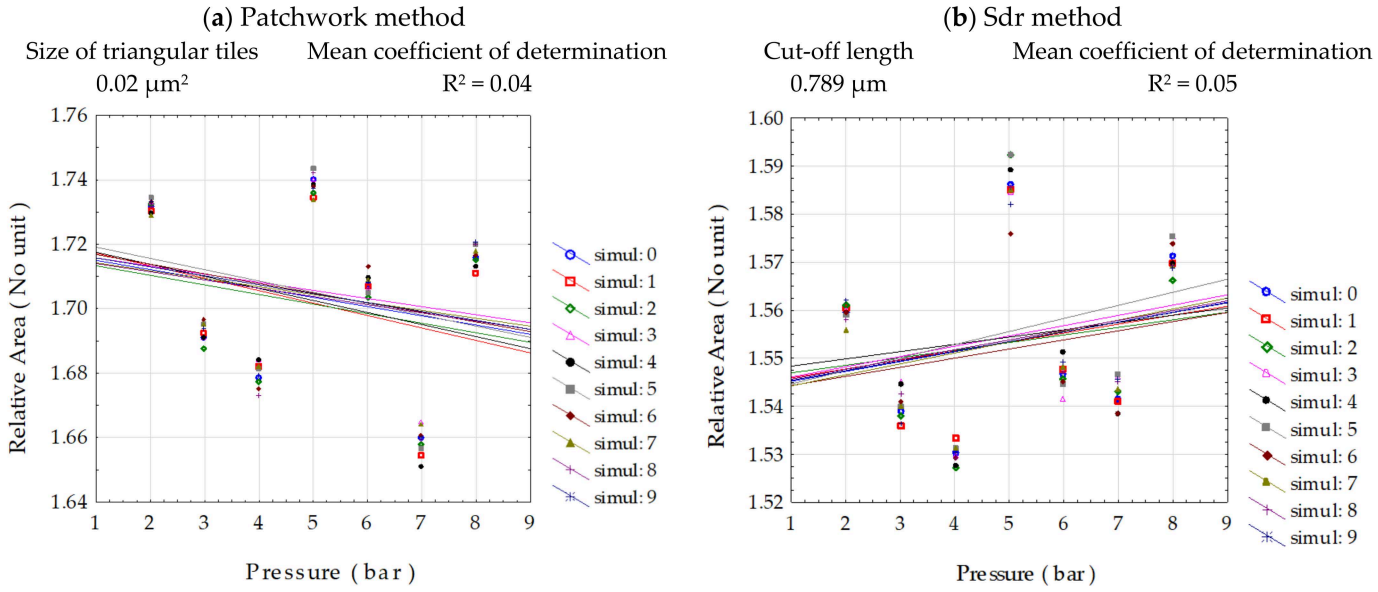

Figure 4. Results of the linear regressions of the relative area as a function of pressure for the two calculation methods. Simulations from 0 to 9 are obtained from bootstrapping replication of the real data and then averaged. The results come from measurements performed on surfaces blasted with the C 300 medium (corundum). Each simulation corresponds to an R^2 value, which is then averaged.

In this study, two statistical hypotheses are formulated to test the effect of blasting pressure on the relative area of surfaces. The null hypothesis (H0) states that there is no significant relationship between the blasting pressure and the relative area of the surfaces, implying that any observed variation may be attributed to random chance. In contrast, the alternative hypothesis (H1) proposes that a significant relationship exists between these two variables, suggesting a measurable impact of pressure on surface topography. These hypotheses are statistically tested to determine whether the data provide sufficient evidence to reject H0 and accept H1.

For H0, the data were permuted to represent the distribution of regression coefficients if there was no real relationship between the pressure and the relative area. This means that for each combination of the relative area (RA) and pressure, there are 7 pairs of data. In the bootstrapping for H0, the seven values of relative area are randomly permuted. This means that instead of using the actual order of the relative area on every scale, such as X_1 to X_7, and the 7 pressure values Y_1 to Y_7, we create new combinations of pairs to calculate the coefficient of regression by performing a random permutation of Y_1 to Y_7. The goal is to generate a distribution of R^2 that could be obtained if pressure and relative area were not correlated. Although this method can eliminate any apparent correlation between pressure and relative area, it is important to note that the regression coefficients obtained will not be exactly equal to zero.

To compare these hypotheses robustly, three bootstrapping protocols have been defined: simple bootstrap, double bootstrap based on pairs, and double bootstrap based on residuals.

2.4.2. Simple Bootstrap

The relationship between the blasting pressures (independent variable) and the developed surface area (dependent variable) using 50 topography measurements for each of the seven different pressures (ranging from 2 to 8 bar) is investigated. Our goal is to assess

how well the variation in pressure explains the variation in the developed surface area, which will be quantified using the regression coefficient R^2.

Data Preparation and Bootstrapping Sampling

We have seven blasting pressures (e.g., 2, 3, 4, 5, 6, 7, 8 bar). For each pressure, there are 50 measurements of relative area. For each measurement, a bootstrapping is performed as follows:

1. For each pressure level (2, 3, . . ., 8 bar), conduct the following:
   - Draw 50 random samples with replacement from the 50 original measurements for that pressure level;
   - Calculate the mean relative area for that resample;
   - Repeat this process multiple times (e.g., 1000 times) to obtain a distribution of bootstrapping means for each pressure.
2. For each of the 7 pressures, end up with a set of means from the bootstrapping means.

Regression Analysis for Each Resampling

With a set of bootstrapping means for each pressure level, conduct the following:

- Perform a linear regression between the pressure (independent variable) and the corresponding bootstrapping mean surface relative area (dependent variable).
- Calculate the coefficient of determination R^2 for this regression. The R^2 value will tell us how much the variation in the developed surface area is explained by the variation in the grit blasting pressure.
- Repeat the entire bootstrapping resampling process many times (e.g., 1000 times).

Each time, a new set of regression results and a new R^2 value are obtained. By repeating this process, a distribution of R^2 values is created.

Analysis of the R^2 Distribution

Once the distribution of R^2 values is obtained, conduct the following:

- Calculate the mean or median of the R^2 values to obtain an overall sense of the fit;
- Estimate confidence intervals (e.g., 95% CI) for R^2, giving a range in which the true relationship between the pressure and the surface area likely lies;
- Assess the stability of the relationship by looking at the variability in the R^2 values across the bootstrapped samples.

2.4.3. Double Bootstrap Based on Pair Replication

The relationships between the blasting pressure and the developed surface area are analyzed by using a two-stage bootstrapping approach. In the first stage, the surface area measurements for each pressure are resampled, and in the second stage, a pairwise bootstrap on the resulting bootstrapping means is performed. The goal is to explore the statistical distribution of the regression coefficient R^2, providing a more robust understanding of the relationship. In this extended approach, we perform two levels of bootstrapping:

1. A first bootstrap on the individual surface area measurements for each pressure level;
2. A second bootstrap on the pairs [pressure, surface area means] derived from the first bootstrap.

By incorporating the second bootstrap, the variability is determined not only within each pressure group but also in the overall relationship between the pressure and the developed surface area.

Data Preparation

As previously specified, we have seven grit blasting pressures, each with 50 topography measurements of developed surface area. Two bootstrapping levels are performed.

First-Level Bootstrap

For each pressure, a simple bootstrap is performed, resulting in a set of bootstrapping means for each of the 7 pressure levels whose means are input for the next stage.

Second-Level Bootstrap: Bootstrap on Pairs

Once we have the bootstrapping means for each pressure, we introduce the second bootstrap step, where we resample pairs [pressure, bootstrapping means]:

1. Resample pairs: for each iteration, randomly sample pairs [pressure, bootstrapping mean] from the set of 7 pressure levels (with replacement). For example, a bootstrap sample might be [2 bar, mean2], [3 bar, mean3], . . ., [8 bar, mean8].
2. Perform a linear regression: perform a linear regression on the resampled pairs, with pressure as the independent variable and the corresponding bootstrapping mean surface area as the dependent variable.
3. Calculate R^2: for each resampled pair, calculate the regression coefficient R^2, which measures how much the variation in surface area is explained by the variation in pressure.
4. Repeat: repeat this entire second-level resampling process many times (e.g., 1000 times) to build a distribution of R^2 values.

2.4.4. Double Bootstrap Based on Residuals

This is also a two-level bootstrapping method. This time, instead of performing a bootstrap on pairs [pressure, surface area mean], a bootstrap on residuals in the second stage is used. The two methods are similar in concept, but they differ in the way they handle resampling in the second stage. The bootstrap on residuals focuses on the variability captured by the regression model errors, while the bootstrap on pairs resamples the entire dataset. The main difference between the two methods lies in the resampling approach:

- The bootstrap on pairs resamples all the pairs [pressure, surface area mean], which can distort the relationship between the independent (pressure) and dependent (surface area) variables;
- The bootstrap on residuals preserves the structure of the data by resampling only the errors (residuals) of the model, ensuring that the overall relationship between the pressure and the surface area is maintained while introducing variability based on the model accuracy.

First-Level Bootstrap

The first stage remains identical in both approaches, i.e., the following is a simple bootstrap:

1. The surface area measurements within each pressure group (e.g., 50 samples with replacement) are resampled;
2. For each pressure level (2 to 8 bar), the bootstrapping mean is computed;
3. This process is repeated (e.g., 1000 times) to obtain a distribution of bootstrapping means for each pressure level.

After this first step, there is a set of bootstrapping means for each pressure level, just like in the bootstrap on pairs method.

Second-Level Bootstrap: Bootstrap on Residuals

In the bootstrap on pairs method previously described, the following is true:

- All the pairs of pressure and bootstrapping means are resampled;
- For each iteration, the pairs from the set of pressure levels and their corresponding bootstrapping means are sampled randomly (with replacement);
- Then, a new linear regression is calculated, and the regression coefficient R^2 is determined.

In the bootstrap on residuals method, instead of resampling pairs, the following steps are performed:

1. Fit an initial regression: After calculating the bootstrapping means for each pressure level, we fit a linear regression between the pressure (independent variable) and these bootstrapping means (dependent variable). We then calculate the residuals, which represent the differences between the actual bootstrapping means and the predicted values from the regression model.
2. Resample residuals: Instead of resampling pairs, the residuals are resampled with replacement. These residuals capture the variability in the relationship between the pressure and the surface area.
3. Generate new data: For each pressure level, we create new bootstrapping means by adding the resampled residuals to the predicted values from the original regression model (Equation (2)). This step maintains the core structure of the original regression model, ensuring that the relationship between the pressure and the surface area remains intact, while introducing variability based on the residuals.

$$new\ mean = predicted\ value + resampled\ residua \quad (2)$$

4. Perform regression and calculate R^2: We fit a new linear regression to the original pressure values and the newly generated bootstrapping means. The regression coefficient R^2 for this resampled dataset is calculated.
5. Repeat the process (e.g., 1000 times) to generate a distribution of R^2 values, just as we performed in the bootstrap on pairs method.

3. Results

After generating the data with our three bootstrapping protocols, the best protocol for finding the relevant scale to characterize the relationship between relative area and grit blasting pressure can be identified.

Figure 5 presents the results of the R^2 distributions as a function of the scale for the relative area calculation, for the three bootstrapping methods previously described. The bootstrapping methods indicate that regardless of the calculation method or the medium used, the relevance of the R^2 values at scales is given.

For the three bootstrapping methods (Figure 5i–iii), regardless of the media (Figure 5c,e,g), the maximum relevance which highlights the influence of pressure is obtained for a tile size of around 10,000 μm^2 for the Patchwork method and a cut-off length of around 120 µm for the Sdr method (Figure 5a). The choice of this specific cut off is directly tied to the analysis in Figure 5. The box plots included in these graphs allow us to directly observe the variation in the R^2 values with changes in the cut-off parameter. Consequently, a 120 µm cut off and 10,000 μm^2 triangular tile size were chosen as a balance between capturing relevant surface features and minimizing noise while ensuring comparability between the two methods. To determine if the R^2 values associated with this relevance are significant to validate H1, we must look at the distribution of the R^2 values under H0 (Figure 5b).

Figure 6 presents a visualisation of the surface topography after being filtered on the relevant scale for the Sdr Method (120 µm cut off length). Surface are smoother than the original ones but have differences depending on the pressure, the surface blasted at 2 bar is more homogeneous than the two other ones.

The distributions under H0 (Figure 7b) indicate that at a 95% threshold, the R^2 values are located at different points depending on the bootstrapping method used. For the simple bootstrap (Figure 7i), the threshold value is 0.59, indicating that 95% of the values must be below this to invalidate H0. For the paired bootstrap (Figure 7ii), the threshold value is 0.91, and for the residual bootstrap (Figure 7iii), it is 0.83. This assumption is valid for both methods of calculation. These checks under H0 are necessary because the H1 hypothesis alone is not sufficient, considering that the values are correlated if we assume that the surfaces are the same at different filtering scales. For H1, the graphs clearly indicate that the values generally approach 1 regardless of the bootstrapping method used (Figure 7a).

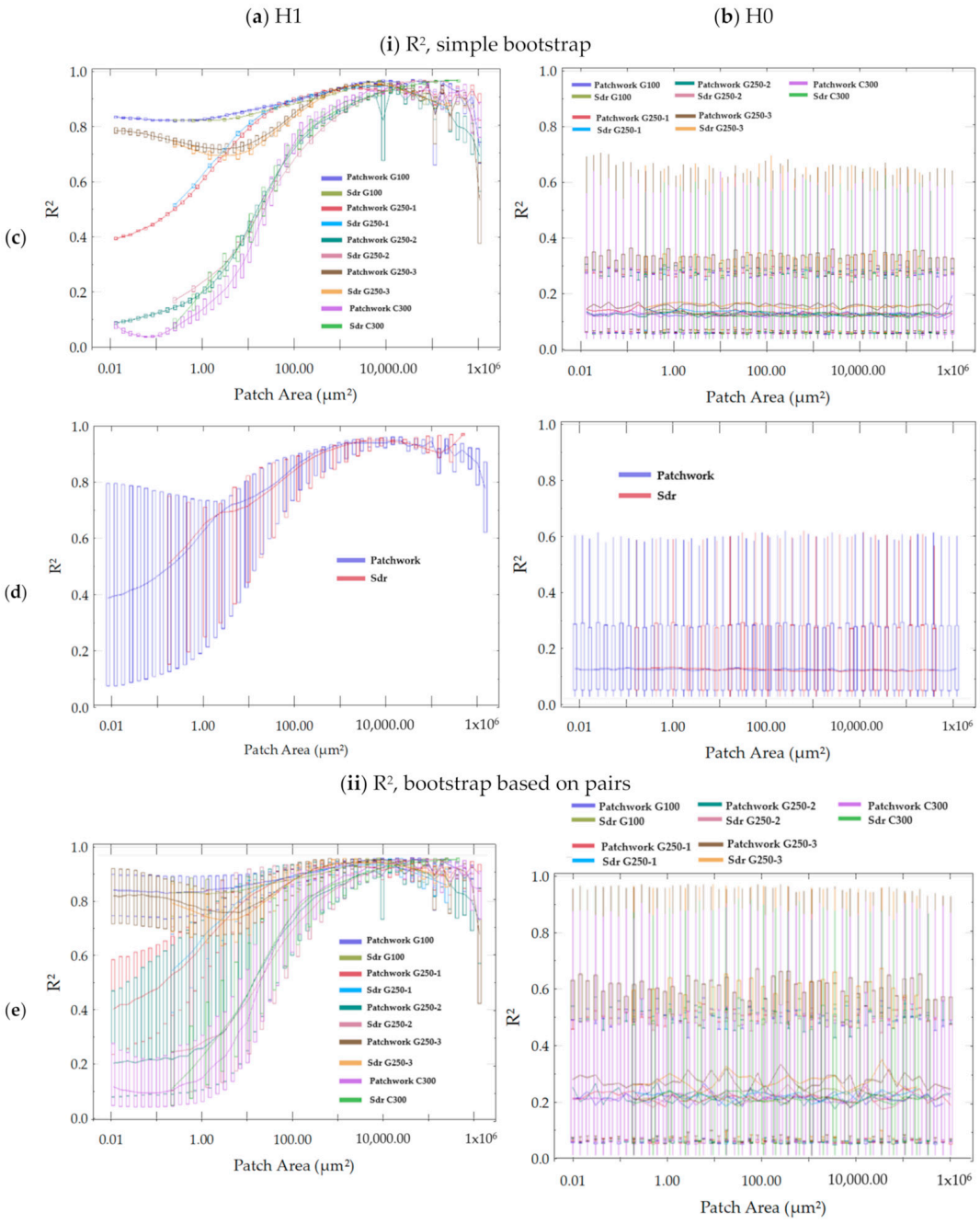

Figure 5. *Cont.*

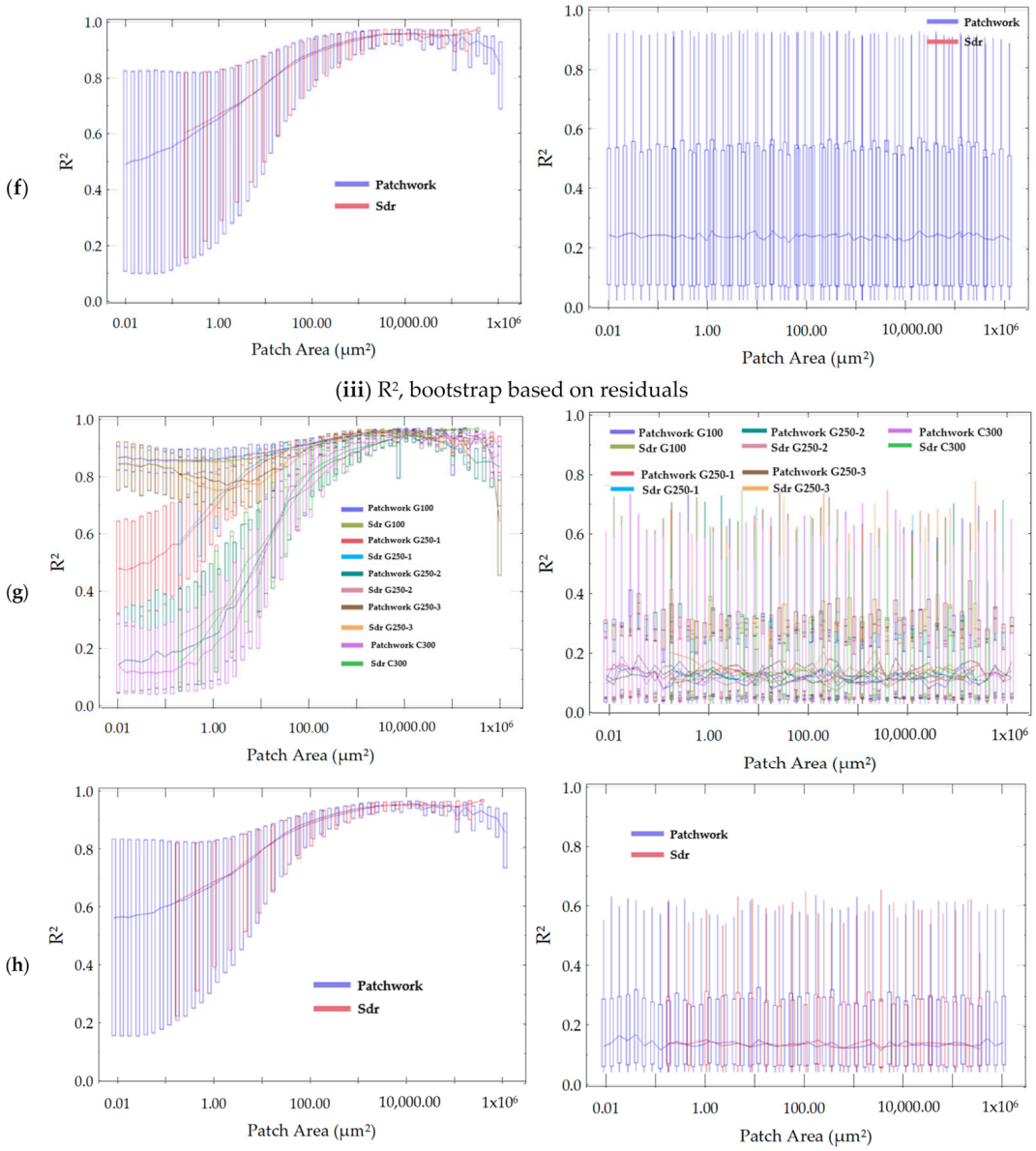

Figure 5. Analysis of the R^2 distributions according to the scale of calculation for relative area under hypotheses H1 (**a**) and H0 (**b**) for the three bootstrapping methods: simple bootstrap (**i**), bootstrap based on pairs (**ii**), and bootstrap based on residuals (**iii**). The tile size of the Patchwork method (in μm^2) is equal to half the square of the cut-off length of the Sdr method. Two plots are proposed for each bootstrapping method: the first one based on the media (**c**,**e**,**g**) and the second one based on the method of the relative area calculation, Sdr or Patchwork (**d**,**f**,**h**).

To continue the analysis, the choice was made to use bootstrapping on residuals as a promising method. Indeed, the threshold for the simple bootstrap, equal to 0.59, is too low under H0 to be helpful to validate significance. Additionally, to capture the variations in the initial model and gain a better view of the uncertainties, the bootstrap based on pairs is too high with a threshold of 0.91. The bootstrap on residuals preserves the original regression structure by resampling residuals, maintaining the relationship between grit pressure and relative area, unlike the paired bootstrap, which may introduce noise or trends. It captures variability from model errors without distorting the data, ensuring that subtle roughness variations are not overshadowed. Moreover, narrower confidence intervals and more stable R^2 estimates are provided, closely aligning with physical observations, making it the most suitable method for identifying relevant scales.

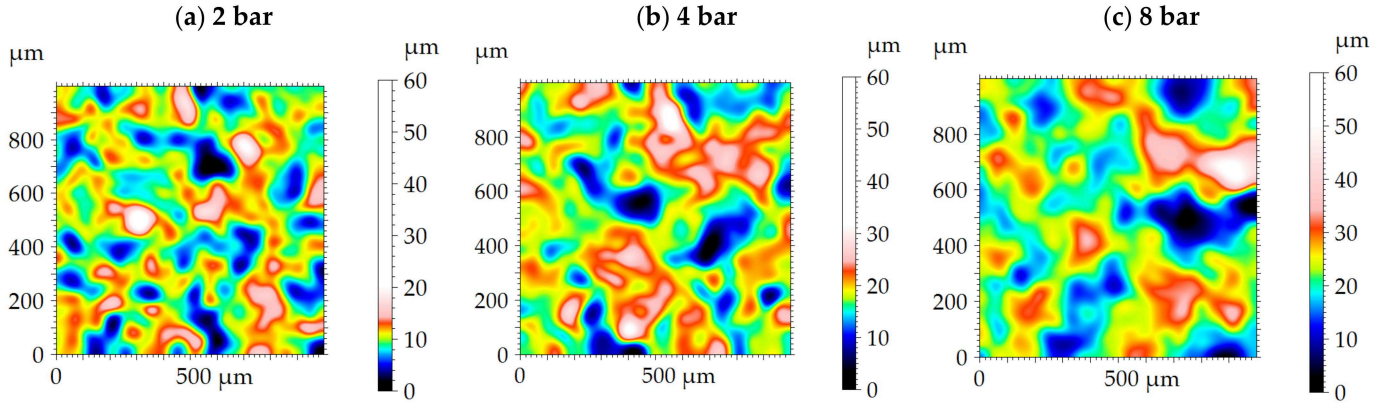

Figure 6. Surface topographies of TA6V samples grit-blasted at 2 bar (**a**), 4 bar (**b**), and 8 bar (**c**) with the C300 medium. The range of height varies significantly. The surfaces are the same as those presented in Figure 2 but this time filtered with a low-pass Gaussian filter at a 120 µm cut off (the relevance scale).

In Figure 8, the slopes (Figure 8i) and intercepts (Figure 8ii) of the bootstrapping model based on residuals for the two methods of calculation (Patchwork and Sdr) are analyzed. For G 100, the relationship between slope stability and initial roughness (Figure 8(ai)) is relatively stable, with smoother and more homogeneous surfaces showing lower variability in slope values. In contrast, for C 300, the relationship is more variable, with higher initial roughness leading to increased unstable slope values due to the angular particles' sharp edges. The variations stabilize at the same scale as in the comparison of the bootstrapping models in Figure 5 under H1. The results of the slope and intercept variations show a distinct behavior for the C 300 blasting medium (corundum). For this aggressive medium, at small calculation scales, there is little variation in the surface area developed relative to pressure. The high intercept at small scales indicates that even at the lowest pressure, the surface is already rougher compared to other media. The results of all the distributions of slopes and intercepts can be found in Appendix B.

After selecting our bootstrap on residuals model, the analysis of the R^2 distribution at the relevant scale using this method shows disparities among the media and methods of calculation (Figure 9). Surprisingly, the trend is reversed for the R^2 values compared to the methods of calculation of the relative area. The Patchwork method (Figure 9i) shows numerous values close to 1 for G 100, the third series of G 250, and C 300 media, whereas the Sdr method (Figure 9ii) shows values close to 1 for series 1 and 2 of the G 250 medium (Figure 9a). While both methods yield high R^2 values, there are notable differences between them. The Patchwork method produces smoother histograms, which may be advantageous for certain analyses. However, in the case of the triple repetition for the same medium G 250, the results differ between the two methods, making it challenging to establish a definitive strategy for selecting one method over the other. To address this, the method yielding the highest correlation (the best R^2 value) could be prioritized. This strategy combines the strengths of both methods while ensuring the most robust correlation for each specific case.

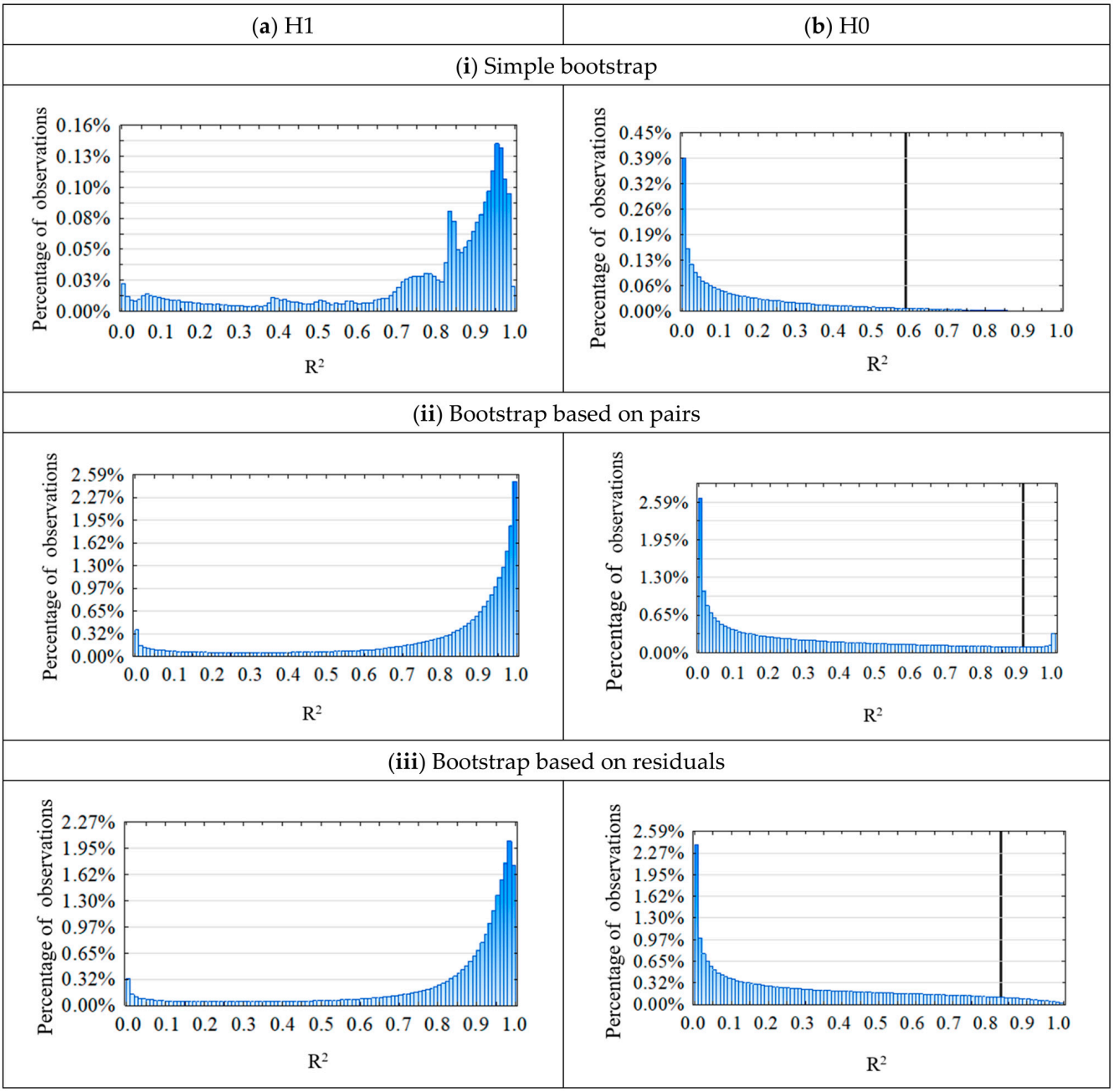

Figure 7. Distributions of the R^2 values at all scales under H1 (**a**) and H0 (**b**) for every method of bootstrapping computation: simple bootstrap (**i**), paired bootstrap (**ii**), and bootstrap based on residuals (**iii**). The black lines on the H0 plots are the threshold value at 95% of the R^2 distribution: 0.59 (**bi**), 0.91 (**bii**), and 0.83 (**biii**).

To conclude this analysis, the results of the relationship between relative area and pressure were plotted at the optimal pertinence scale (Figure 9), encompassing all media (Figure 10a–e) and both relative area calculation methods (Figure 10i,ii). The relevance scale ranges between 10,000 μm^2 and 14,000 μm^2 for the Patchwork method (Figure 10i).

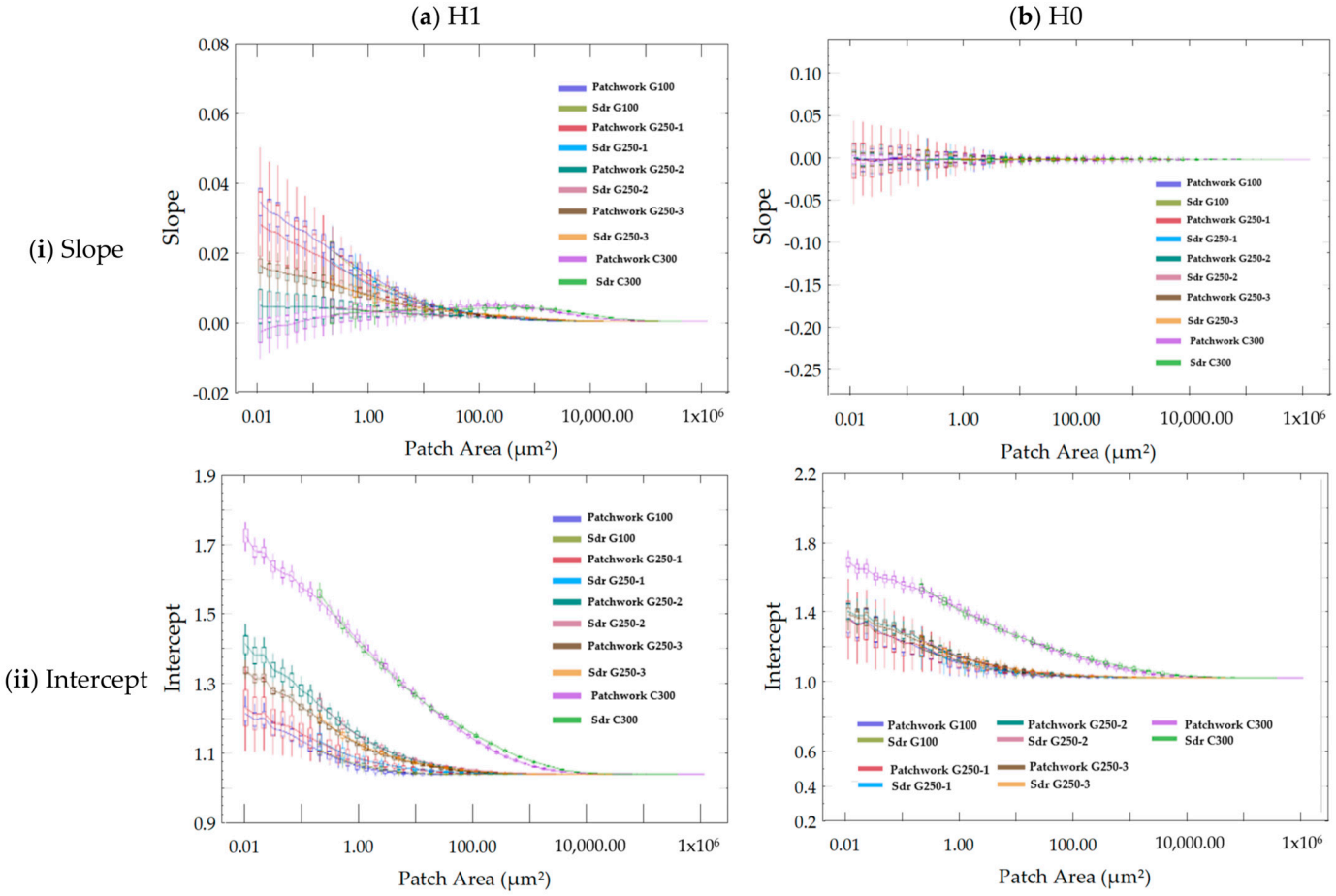

Figure 8. Evolution of the slope (**i**) and intercept (**ii**) as a function of scale for H1 (**a**) and H0 (**b**) using bootstrap based on residuals.

The study of the distribution of the intercepts according to the slopes at the relevant scale can be added to these insights (Figure 11). Besides the fact that the glass beads (G100, G250) are grouped together, there are three types of distributions of these points. The first one is a rather oblique distribution of intercepts for the fine glass beads (G 100). The slightly oblique distributions of this material indicate that the intercept is relatively constant, while the slope varies, suggesting that the initial roughness is quite stable, but the effect of pressure varies. While the points form a nearly vertical distribution for the angular medium (C 300), the effect of the pressure on the relative area (slope) is quite stable for this medium, but the initial roughness varies significantly. This type of distribution could indicate that the medium had a uniform relation to the pressure but with variable starting conditions. These findings suggest that using an angular medium like C 300 might be optimal for applications requiring high stability in response to varying pressures. The variability in surface roughness across the different media (e.g., G 100, G 250, C 300) can be attributed to the intrinsic properties of each medium, including particle hardness, size, and morphology. For instance, the corundum-based C 300 medium, characterized by its higher hardness and angular morphology, induces more aggressive impacts on the surface, resulting in a higher intercept at small scales. It indicates a rougher initial surface even at lower pressures compared to the softer and more spherical glass beads (e.g., G 100 and G 250). In contrast, the glass beads, due to their lower hardness and smoother shape, tend to cause more gradual surface roughening, leading to lower initial roughness and a more pronounced dependency on pressure, as seen in their slope distributions. The differences in particle size also play a role: larger particles (e.g., G 250) can create broader indentations, contributing

to different scaling behaviors compared to smaller particles like G 100. These intrinsic properties directly influence the interaction mechanisms between the blasting media and the surface, which are captured in the variations in the slope and intercept distributions, reflecting the distinct roughness evolution patterns for each medium. However, the two methods of calculation, Patchwork and Sdr, lead to the same three clusters in Figure 11, which means that both methods characterize the relevant scale for studying the relative area depending on the pressure of blasting.

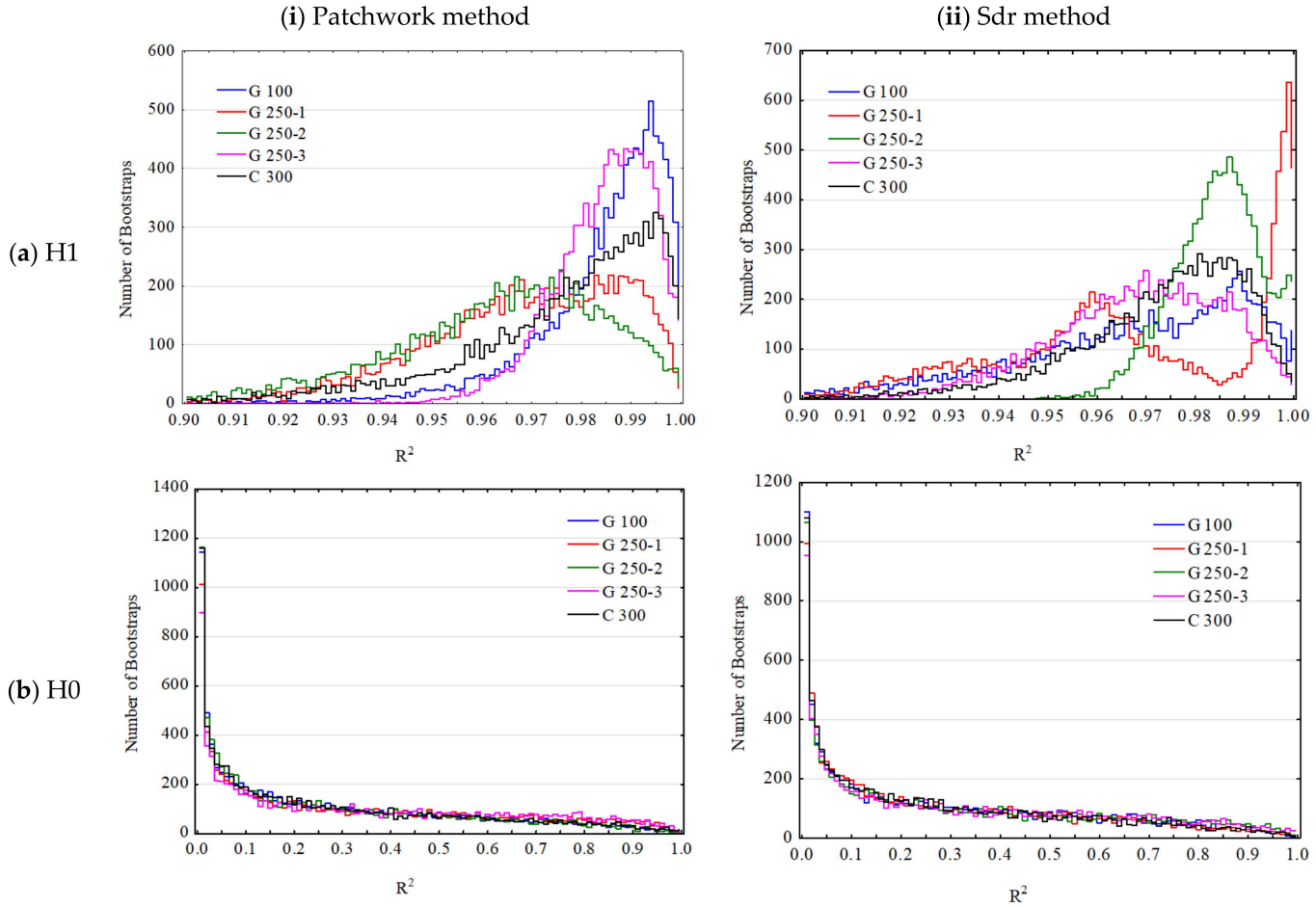

Figure 9. Distribution of the R^2 values by medium at the relevant scale for the Patchwork (**i**) and Sdr (**ii**) methods and for H1 (**a**) and H0 (**b**). The digits after 250 indicate the blasting series (e.g., G 250-1 = first series of the G250 medium).

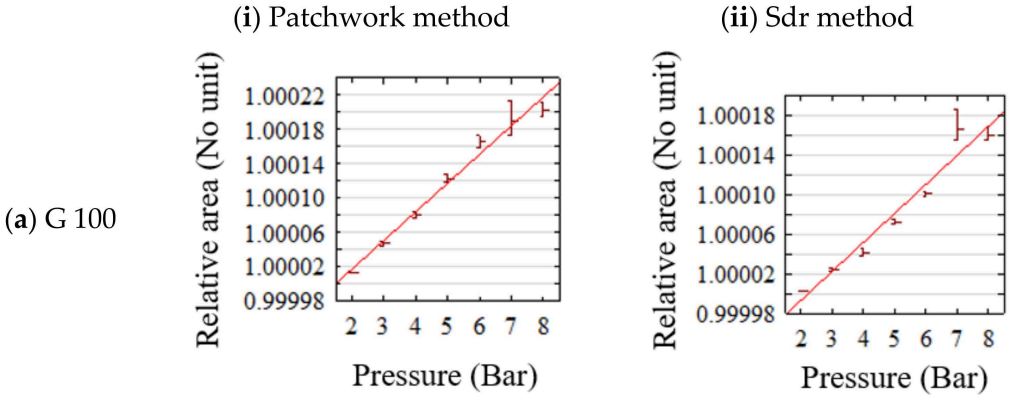

Figure 10. *Cont.*

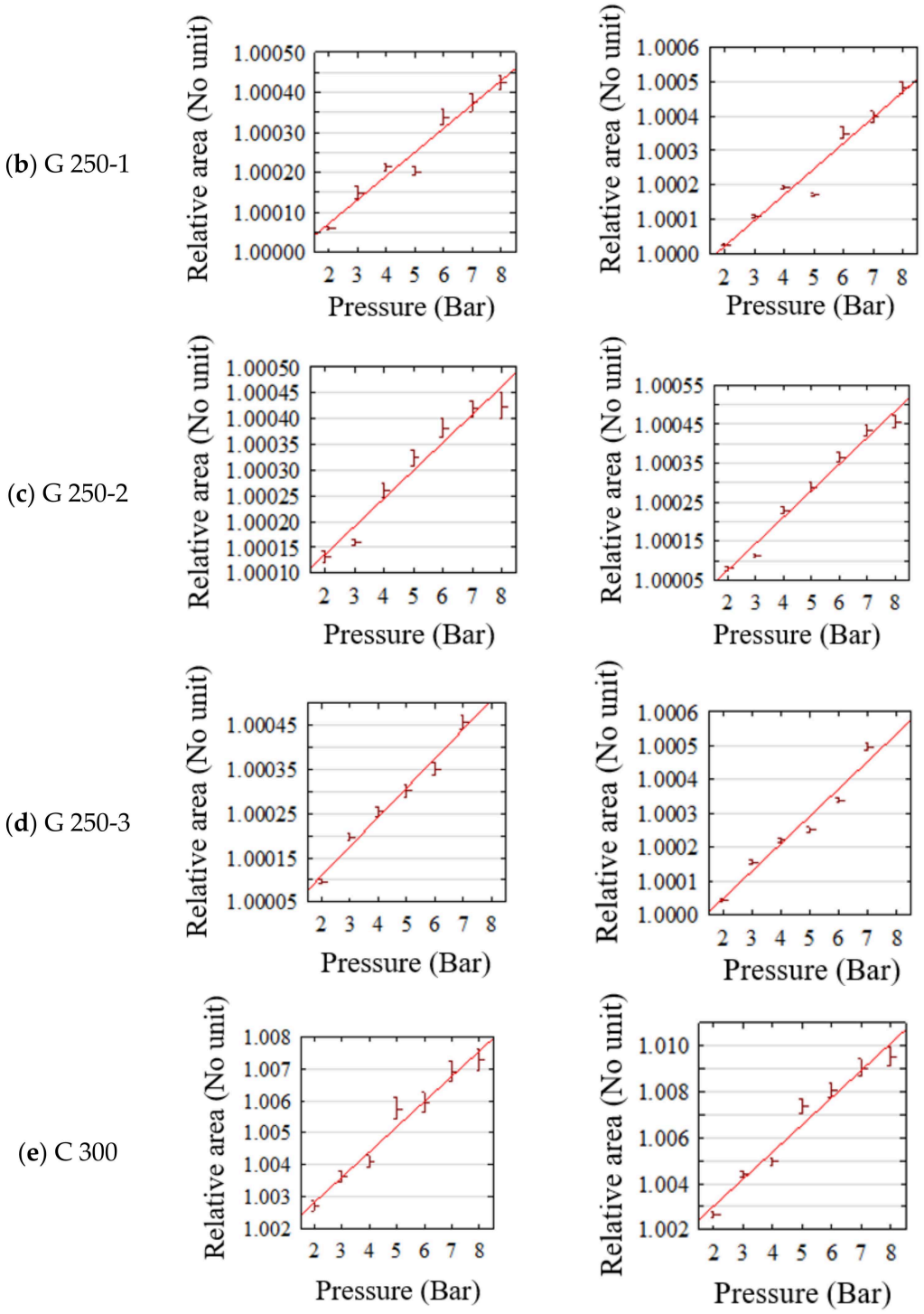

Figure 10. Box plots of the relative area values by pressure at the relevance scale (tile size between 10,000 μm^2 and 14,000 μm^2 for the Patchwork method and cut-off length of 120 μm for the Sdr method). The results are presented by medium (**a**–**e**) and calculation method (**i**,**ii**).

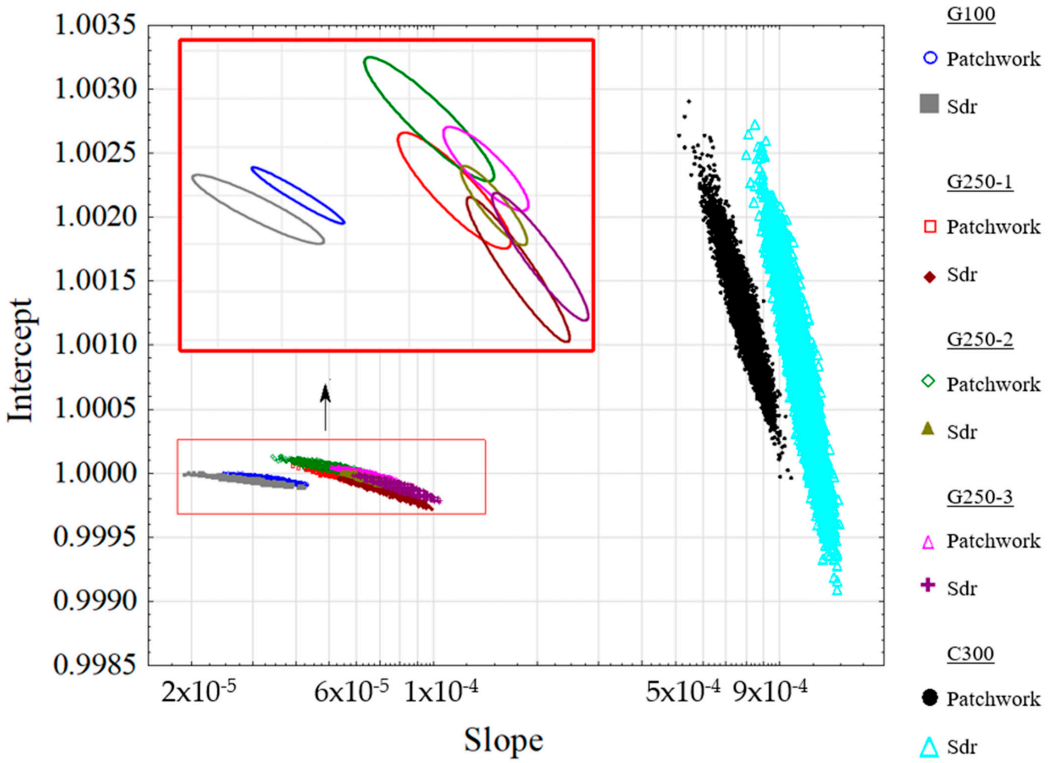

Figure 11. Bivariate density (intercept, slope) of the linear regression at the relevant scale between relative area for the three media of grit blasting and the two methods of relative area calculation (Patchwork, Sdr) obtained by bootstrap on residuals. The red frame is a zoom with ellipses of confidence at 95%.

4. Discussion

The analysis results indicate that the bootstrapping method based on residuals is the best choice for characterizing the relevance scale to highlight the influence of the grit blasting pressure on the relative area. In this study, we have several aspects that warrant comparison with the existing literature. These aspects pertain to roughness parameters, specifically how our method is innovative compared to the grit blasting characterization parameters already presented in the literature and the scale used to characterize the surface. This also concerns the different media and how their nature influences surface topography.

The use of the Sa parameter to characterize the influence of blasting on materials is documented in the literature [10]. However, the methods of calculation of the relative area proposed in this study is considered more suitable because the relative area captures surface irregularities at different scales and is sensitive to large-scale features such as deep recesses and significant local variations. The Sdq parameter is discussed in the study of Ho et al. [15]. Impact craters are generated by SiC particles striking the surface of the substrate. The repetitive impacts can lead to the development of a plastically deformed layer and the formation of additional craters on top of existing ones. This process results in the creation of a series of small peaks and valleys with sharp edges, whose slopes can be characterized using Sdq. This study, which is very similar to ours, gives a scale of relevance for characterizing the relationship between the value of the multiscale Sdq parameter and the blasting pressure. The filtering uses a low-pass filter with a cut off of 120 µm, which also corresponds to our relevance scale with the Sdr method. This result is interesting because the pressures used for this study changed slightly, ranging from 1 to 7 bar, whereas our samples were blasted from 2 to 8 bar. This comparison gives an argument for the generalization of our results.

It is essential to address two critical aspects in the discussion part: the influence of surface modification during the experiment on the results and the impact of the chosen Gaussian filtering method on fractal surfaces. Below, we provide detailed considerations regarding these aspects. Factors such as humidity and temperature can disrupt measurements by introducing uncertainties. The room where the measurements were conducted is a temperature-controlled environment with an automatic regulation system maintaining a constant temperature of 20 °C. Regarding humidity, the air circulation provided by the ventilation system helps regulate condensation and the humidity density in the measurement room. Neither the temperature of the metal during blasting nor the humidity altered the surface appearance during the experiment due to the excellent mechanical properties of TA6V, which is resistant to heat and corrosion [26,27,47]. Regarding the use of Gaussian filtering, two remarks can be made. This surface filtering method is the most common in surface processing; it is well documented, and its limitations are well known. However, we acknowledge that for fractal surfaces, such as those generated by blasting, distortions may be introduced by the Gaussian filter on the sharpest features. The chapter on the use of filters in the book by Blunt and Jiang [36] clearly explains the difference between robust and Gaussian filters on a plateau-honed surface. However, the robust filter requires a longer computation time, which explains our choice in this study. A comparison between both is necessary.

The results indicate that the relationship between pressure and roughness evolution is not strictly linear for some blasting media such as C300, as initially hypothesized. At lower pressures (e.g., 2 bar), roughness increases are moderate and uniform, reflecting gradual material erosion. In contrast, at higher pressures (e.g., 8 bar), the changes become pronounced, with deeper asperities and irregular textures, likely due to enhanced impact energy and its effects on asperity deformation and void formation.

Given these results, a nonlinear model such as $Y = aP^b + c$ may better capture the relationship between pressure and roughness, where Y represents a roughness parameter, P is the pressure, and a, b, c are the model parameters. Notably, the model converges to the linear approximation $Y = aP + c$, as discussed earlier in this article, when b is statistically equal to 1. Significant deviations from $b \approx 1$ could reveal transitions in the dominant mechanisms of surface modification with different materials and process conditions.

To test if $b < 1$, $b = 1$ *or* $b > 1$, the bootstrapping techniques proposed in this paper (simple, paired, or residual bootstraps) could assess the statistical significance of parameters a, b, and c, providing insights into the interplay between the pressure, media type, and substrate response. However, implementing such a nonlinear model would require solving a regression problem through iterative optimization algorithms, ensuring convergence to a unique global minimum. This added complexity would extend beyond the current study's scope. We plan to apply this framework to further research on the nonlinear effects of contact pressure and media type on surface topography.

The grit blasting process is known to exhibit inherent variability, which can contribute to the inconsistencies observed in the G 250 medium series. Factors related to the sandblasting equipment itself, such as nozzle wear or inconsistent abrasive flow, can further contribute to variations in surface preparation. These variations lead to fluctuations in the surface roughness and texture of materials treated with G 250, as the process may not consistently achieve the intended surface finishing across different batches or applications. Therefore, the lack of reliability in the grit blasting process is likely a significant factor contributing to the variability observed in the G 250 series.

The results of this study may encourage further research to continue determining the reference scale of complex surfaces created by different processes that allow for varying intensities of surface modification. Thus, it is possible that the results could be

compared with acid etching, electric discharge machining, and shot peening (i.e., steel bead blasting) on titanium alloys like in this study. By varying parameters such as the type of filament used and the electrical intensity [48] for electric discharge machining, it is possible to modify the surface topography and study the relevant scale for this process. The same applies to soaking time in acid during chemical etching [49]. Some studies on functional optimization already exist and aim to identify a relevant scale for process analysis. For instance, one study highlights the sensitivity of hMSC cells to topographical features at different scales (Ra, Sm) on surfaces generated by EDM (electric discharge machining) [50].

5. Conclusions

In this study, the results of different bootstrapping methods are presented in order to find a relevant scale for determining the relationship between the relative area and blasting pressure. Three types of media were tested with seven pressures. Two methods for calculating the relative area (Patchwork and Sdr) and three bootstrapping methods (simple bootstrap, double bootstrap based on pair replication, and double bootstrap based on residuals) for determining the relevant scale associated with the regression are studied. Several factors already presented in other studies were considered to generalize our results, such as the influence of different media or different pressures. The scale of pertinence corresponds to a tile size of 10,000 μm^2 for the Patchwork method and a filtering cut-off length of 120 μm for the Sdr method using low-pass filtering. Using the regression results of the bootstrap on residuals method, the R^2 value required to characterize the area/pressure link has to be higher than 0.83 to be significant at the threshold of 5%. In addition, to determine pertinent scales and the R^2 values, our study contributes to the understanding of how different media types and blasting pressures influence surface topography, providing insights that can inform more effective material processing and surface treatment strategies.

Author Contributions: Conceptualization, M.B.; methodology, C.B.; software, R.G.; validation, M.B. and M.W.; formal analysis, M.B. and F.B.; investigation, F.B. and J.L.; data curation, J.L. and F.B.; writing—original draft preparation, F.B.; writing—review and editing, J.L. and F.B.; visualization, M.B. and F.B.; supervision, M.B. All authors have read and agreed to the published version of the manuscript.

Funding: This research received no external funding.

Data Availability Statement: The data are available on demand.

Conflicts of Interest: Author Julie Lemesle was employed by U.R Concept. The remaining authors declare that the research was conducted in the absence of any commercial or financial relationships that could be construed as a potential conflict of interest.

Appendix A

The original unfiltered blasted surface topographies with the three materials used in this study are presented at different pressures (in bar) to represent the differences between topographies.

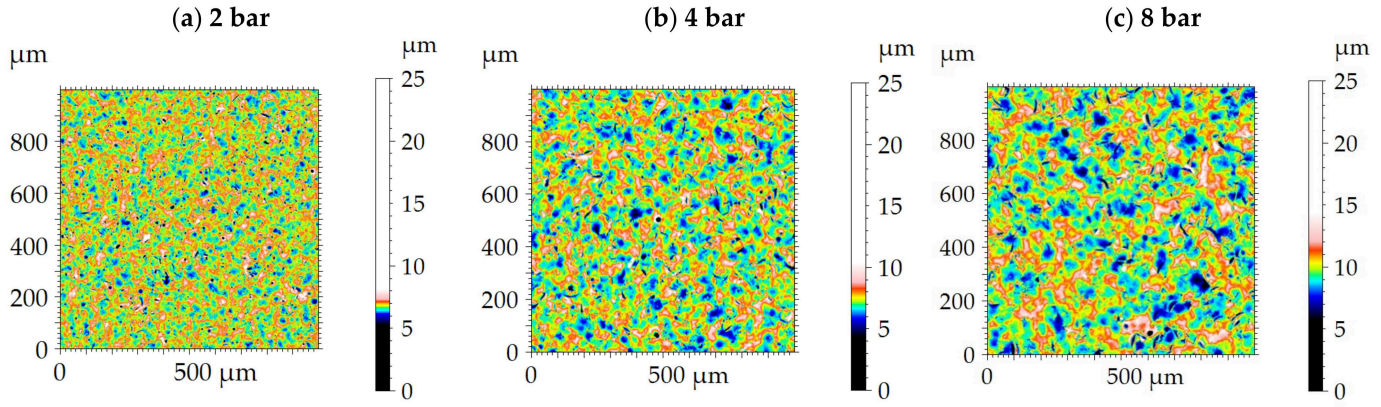

Figure A1. Surface topographies of blasted surface using the medium G 100 at (**a**) 2 bar of pressure, (**b**) 4 bar of pressure, and (**c**) 8 bar of pressure.

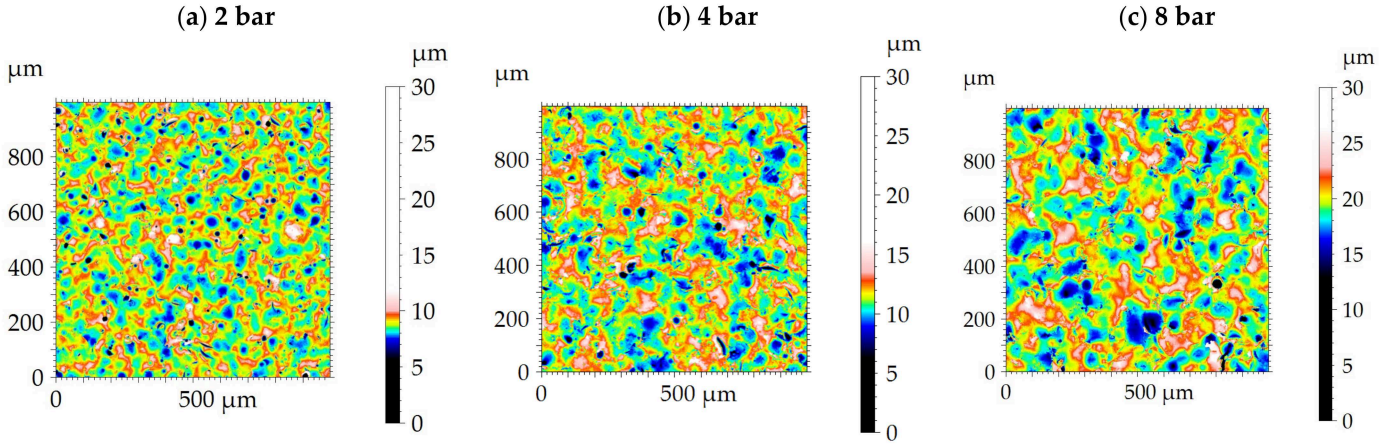

Figure A2. Surface topographies of blasted surface using the medium G 250 at (**a**) 2 bar of pressure, (**b**) 4 bar of pressure, and (**c**) 8 bar of pressure.

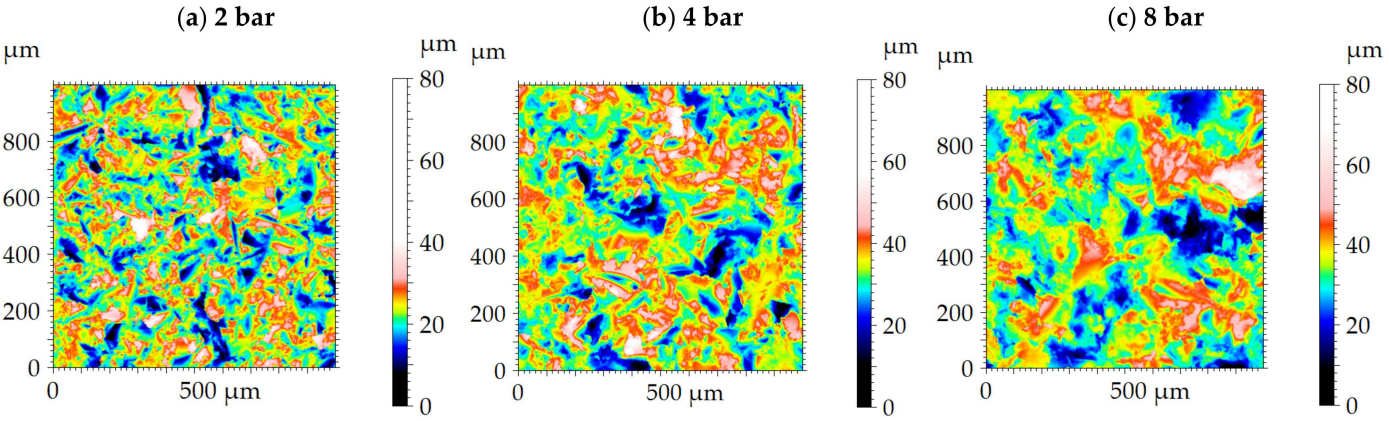

Figure A3. Surface topographies of blasted surface using the medium C 300 at (**a**) 2 bar of pressure, (**b**) 4 bar of pressure, and (**c**) 8 bar of pressure.

Appendix B

This section presents tables containing the results of linear regressions according to each hypothesis and each bootstrapping method.

Table A1. Results of the linear regression distributions according to hypothesis H1 for the simple bootstrap method. For the G 250 medium, the last digit represents the series, e.g., G 250-1 corresponds to the first series of this medium.

Media	Intercept P5	R^2 P5	Slope P5	Intercept P50	R^2 P50	Slope P50	Intercept P95	R^2 P95	Slope P95
					Patchwork method				
G 100	0.99994346	0.9605421	3.1964×10^{-5}	0.99994994	0.98024554	3.3521×10^{-5}	0.99995545	0.99069454	3.5564×10^{-5}
G 250-1	0.99994265	0.93998527	5.6607×10^{-5}	0.99995483	0.95741298	5.9307×10^{-5}	0.99996718	0.97144593	6.2193×10^{-5}
G 250-2	1.00001458	0.91216793	5.0771×10^{-5}	1.00002897	0.94877385	5.4101×10^{-5}	1.00004328	0.97272786	5.7609×10^{-5}
G 250-3	0.99996649	0.96296679	6.356×10^{-5}	0.99997767	0.97724731	6.6341×10^{-5}	0.99998741	0.98845025	6.9056×10^{-5}
C 300	1.00101778	0.93252007	0.00074162	1.00123208	0.96675567	0.00079234	1.00145402	0.98623911	0.00083841
					Sdr method				
G 100	0.99993077	0.91114478	2.8109×10^{-5}	0.99993543	0.95429143	2.9207×10^{-5}	0.99993925	0.97222884	3.0678×10^{-5}
G 250-1	0.99986366	0.94674398	7.2577×10^{-5}	0.99987231	0.95471517	7.4832×10^{-5}	0.99988003	0.95981093	7.7251×10^{-5}
G 250-2	0.99993112	0.96827255	6.6163×10^{-5}	0.99994013	0.97783397	6.8047×10^{-5}	0.99994774	0.98597727	7.0285×10^{-5}
G 250-3	0.99987676	0.94419689	7.9193×10^{-5}	0.99988505	0.95428896	8.1181×10^{-5}	0.99989356	0.96350047	8.3368×10^{-5}
C 300	1.00045608	0.93746278	0.00112675	1.00067672	0.96254004	0.0011778	1.00088318	0.97971935	0.00123367

Table A2. Results of the linear regression distributions according to hypothesis H0 for the simple bootstrap method. For the G 250 medium, the last digit represents the series, e.g., G 250-1 corresponds to the first series of this medium.

Media	Intercept P5	R^2 P5	Slope P5	Intercept P50	R^2 P50	Slope P50	Intercept P95	R^2 P95	Slope P95
					Patchwork method				
G 100	0.99998005	0.00074667	-2.59889×10^{-5}	1.00011303	0.0998969	7.95122×10^{-7}	1.00024542	0.57852645	2.8049×10^{-5}
G 250-1	1.00000187	0.00099695	-0.00005105	1.00024848	0.09622853	5.4433×10^{-7}	1.0004976	0.58899767	4.9761×10^{-5}
G 250-2	1.00006342	0.00116497	-4.19153×10^{-5}	1.00028471	0.09044521	2.79673×10^{-6}	1.00051083	0.55888993	4.5329×10^{-5}
G 250-3	1.00003625	0.00088057	-4.96151×10^{-5}	1.00028404	0.12048242	-1.49483×10^{-6}	1.0005359	0.64680814	4.8274×10^{-5}
C 300	1.0021071	0.0005601	-0.000653803	1.00525864	0.08550533	-1.08371×10^{-5}	1.00840518	0.55558088	0.00063065
					Sdr method				
G 100	0.99996117	0.00153102	-2.35362×10^{-5}	1.00007958	0.10014213	5.07146×10^{-7}	1.00020192	0.58251626	2.3917×10^{-5}
G 250-1	0.99993002	0.00103109	-6.52164×10^{-5}	1.00026373	0.08679445	-3.912×10^{-6}	1.00057789	0.58270044	6.2492×10^{-5}
G 250-2	0.99999004	0.00129898	-5.41773×10^{-5}	1.00029743	0.10132161	-3.3893×10^{-6}	1.00055961	0.56778929	5.7678×10^{-5}
G 250-3	0.99994349	0.00151227	-6.60741×10^{-5}	1.00027356	0.12006613	-4.5955×10^{-6}	1.00057745	0.64192854	6.2393×10^{-5}
C 300	1.00188342	0.00087451	-0.000933592	1.00663373	0.09388461	-1.4159×10^{-5}	1.01112943	0.56925084	0.00091395

Table A3. Results of the linear regression distributions according to hypothesis H1 with the paired bootstrap method. For the G 250 medium, the last digit represents the series, e.g., G 250-1 corresponds to the first series of this medium.

Media	Intercept P5	R^2 P5	Slope P5	Intercept P50	R^2 P50	Slope P50	Intercept P95	R^2 P95	Slope P95
					Patchwork method				
G 100	0.99992846	0.93651857	2.97081×10^{-5}	0.99994992	0.98765361	3.34376×10^{-5}	0.99996945	0.99933642	3.9465×10^{-5}
G 250-1	0.99991799	0.85158765	5.13625×10^{-5}	0.99995367	0.96156467	5.92575×10^{-5}	0.99999982	0.99606657	6.6725×10^{-5}
G 250-2	0.99997389	0.88291308	4.23452×10^{-5}	1.00002549	0.96352655	5.4452×10^{-5}	1.00010307	0.99502698	6.745×10^{-5}
G 250-3	0.99994599	0.94350252	5.19333×10^{-5}	0.99997793	0.98176962	6.61776×10^{-5}	1.00004143	0.99932267	7.3596×10^{-5}
C 300	1.00073813	0.88411381	0.000691077	1.00119264	0.97430649	0.000793964	1.00180254	0.99803303	0.00091091
					Sdr method				
G 100	0.99990288	0.89934141	2.43914×10^{-5}	0.99993617	0.96513054	2.91411×10^{-5}	0.9999516	0.99813461	3.5923×10^{-5}
G 250-1	0.99981818	0.83799507	6.65061×10^{-5}	0.99987617	0.95563311	7.46588×10^{-5}	0.999907	0.99924201	8.2506×10^{-5}
G 250-2	0.9998916	0.95753257	5.96684×10^{-5}	0.99993774	0.98344327	6.85639×10^{-5}	0.99998996	0.99888513	7.859×10^{-5}
G 250-3	0.99982669	0.90361156	5.85351×10^{-5}	0.99988662	0.96528469	8.15432×10^{-5}	0.99997794	0.99853208	9.2672×10^{-5}
C 300	0.99986501	0.90528018	0.001002537	1.00060315	0.97048401	0.001182872	1.00176586	0.99498155	0.00138857

Table A4. Results of the linear regression distributions according to hypothesis H0 with the paired bootstrap method. For the G 250 medium, the last digit represents the series, e.g., G 250-1 corresponds to the first series of this medium.

Media	Intercept P5	R^2 P5	Slope P5	Intercept P50	R^2 P50	Slope P50	Intercept P95	R^2 P95	Slope P95
Patchwork method									
G 100	0.9999	0.00162	−0.000039	1.0001	0.18	−0.0000034	1.0003	0.89	0.000034
G 250-1	0.9998	0.00219	−0.00007	1.0002	0.25	−0.0000005	1.0006	0.89	0.000081
G 250-2	0.9999	0.0022	−0.000071	1.0003	0.22	−0.00000234	1.0006	0.89	0.000067
G 250-3	0.9998	0.00144	−0.000082	1.0002	0.27	0	1.0006	0.96	0.000085
C 300	0.9993	0.00198	−0.001029	1.0052	0.26	0	1.0104	0.91	0.001068
Sdr method									
G 100	0.9999	0.00161	−0.000036	1	0.21	0.0000005	1.0002	0.9	0.000035
G 250-1	0.9997	0.00158	−0.000092	1.0002	0.21	−0.0000014	1.0004	0.89	0.00009
G 250-2	0.9998	0.0014971	-8.77189×10^{-5}	1.0002971	0.2115413	-3.20292×10^{-6}	1.00074429	0.9	0.000083
G 250-3	0.9997	0.0018004	−0.000108688	1.0002212	0.2687166	4.18523×10^{-6}	1.00076864	0.95	0.0001
C 300	0.9991	0.0018053	−0.001491175	1.0071597	0.2177582	−0.000103172	1.0141841	0.8828032	0.001440755

Table A5. Results of the linear regression distributions according to hypothesis H1 with the bootstrap on residuals method. For the G 250 medium, the last digit represents the series, e.g., G 250-1 corresponds to the first series of this medium.

Media	Intercept P5	R^2 P5	Slope P5	Intercept P50	R^2 P50	Slope P50	Intercept P95	R^2 P95	Slope P95
Patchwork method									
G 100	0.999932	0.9565443	3.00899×10^{-5}	0.9999498	0.9874099	3.3551×10^{-5}	0.99996783	0.997883	3.72897×10^{-5}
G 250-1	0.9999097	0.9310252	5.07515×10^{-5}	0.9999556	0.970523	5.93189×10^{-5}	0.99999789	0.9946046	6.75171×10^{-5}
G 250-2	0.9999837	0.9172058	4.52646×10^{-5}	1.0000289	0.9653095	5.42804×10^{-5}	1.00007403	0.992669	6.2665×10^{-5}
G 250-3	0.9999418	0.9660482	5.87297×10^{-5}	0.9999777	0.9854348	6.63596×10^{-5}	1.00001188	0.9970392	7.37881×10^{-5}
C 300	1.0007119	0.9295922	0.000684518	1.0011989	0.9806584	0.000793258	1.00181321	0.9973577	0.000898461
Sdr method									
G 100	0.9999143	0.910487	2.50086×10^{-5}	0.9999348	0.9705346	2.90556×10^{-5}	0.99995929	0.9959154	3.37325×10^{-5}
G 250-1	0.9998133	0.9205808	6.38924×10^{-5}	0.9998784	0.9650501	7.46952×10^{-5}	0.99992171	0.9989289	8.52443×10^{-5}
G 250-2	0.999903	0.9680796	6.14229×10^{-5}	0.9999401	0.9845218	6.83071×10^{-5}	0.99997368	0.9979556	7.49173×10^{-5}
G 250-3	0.9998274	0.9370731	6.85729×10^{-5}	0.9998864	0.9694675	8.09004×10^{-5}	0.9999449	0.9928928	9.30415×10^{-5}
C 300	0.9999004	0.9376534	0.001023062	1.0006449	0.9760935	0.001181016	1.00150702	0.9940184	0.001328685

Table A6. Results of the linear regression distributions according to hypothesis H0 with the bootstrap on residuals method. For the G 250 medium, the last digit represents the series, e.g., G 250-1 corresponds to the first series of this medium.

Media	Intercept P5	R^2 P5	Slope P5	Intercept P50	R^2 P50	Slope P50	Intercept P95	R^2 P95	Slope P95
Patchwork method									
G 100	0.9999299	0.0020084	-3.11653×10^{-5}	1.0001127	0.202859	9.53073×10^{-7}	1.00028281	0.7994261	3.65729×10^{-5}
G 250-1	0.9999497	0.0023251	-7.31388×10^{-5}	1.0002654	0.2443196	-2.80214×10^{-6}	1.00061606	0.8626616	6.14137×10^{-5}
G 250-2	1.0000079	0.001991	-5.11685×10^{-5}	1.000287	0.1917183	2.84894×10^{-6}	1.00056674	0.78524	5.6151×10^{-5}
G 250-3	0.9999356	0.0029693	-6.35342×10^{-5}	1.0002779	0.288483	-6.62178×10^{-7}	1.00059524	0.8713916	6.56124×10^{-5}
C 300	1.0006622	0.0018682	−0.00086555	1.0049848	0.1982778	4.17098×10^{-5}	1.00951576	0.8162126	0.000857372
Sdr method									
G 100	0.9999363	0.0019827	-3.1144×10^{-5}	1.0000939	0.2274792	-2.54905×10^{-6}	1.00024402	0.8072309	2.78718×10^{-5}
G 250-1	0.9998456	0.0026152	-7.49781×10^{-5}	1.0002684	0.2167074	-5.68906×10^{-6}	1.00064383	0.800484	7.44384×10^{-5}
G 250-2	0.999928	0.0022781	-7.96435×10^{-5}	1.0003079	0.2371843	-5.22383×10^{-6}	1.00069378	0.8569223	6.86005×10^{-5}
G 250-3	0.9998214	0.0029229	-7.80835×10^{-5}	1.0002386	0.2563251	1.99542×10^{-6}	1.00066272	0.8536141	8.14062×10^{-5}
C 300	1.0004782	0.0020249	−0.001196388	1.0067009	0.2076762	-2.27189×10^{-5}	1.01303065	0.7983381	0.001178235

References

1. Whitehouse, D.J. *Handbook of Surface Metrology*; Routledge: New York, NY, USA, 2023; ISBN 978-0-203-75260-9.
2. Leach, R. (Ed.) *Characterisation of Areal Surface Texture*; Springer: Berlin/Heidelberg, Germany, 2013; ISBN 978-3-642-36457-0.
3. Chintapalli, R.K.; Rodriguez, A.M.; Marro, F.G.; Anglada, M. Effect of Sandblasting and Residual Stress on Strength of Zirconia for Restorative Dentistry Applications. *J. Mech. Behav. Biomed. Mater.* **2014**, *29*, 126–137. [CrossRef] [PubMed]

4. Anselme, K.; Bigerelle, M. Topography Effects of Pure Titanium Substrates on Human Osteoblast Long-Term Adhesion. *Acta Biomater.* **2005**, *1*, 211–222. [CrossRef] [PubMed]
5. Kim, S.-J.; Kim, T.-H.; Kong, J.-H.; Kim, Y.; Cho, C.-R.; Kim, S.-H.; Lee, D.-W.; Park, J.-K.; Lee, D.; Kim, J.-M. Dual-Scale Artificial Lotus Leaf Fabricated by Fully Nonlithographic Simple Approach Based on Sandblasting and Anodic Aluminum Oxidation Techniques. *Appl. Surf. Sci.* **2012**, *263*, 648–654. [CrossRef]
6. Shen, Y.; Tao, J.; Tao, H.; Chen, S.; Pan, L.; Wang, T. Nanostructures in Superhydrophobic Ti6Al4V Hierarchical Surfaces Control Wetting State Transitions. *Soft Matter* **2015**, *11*, 3806–3811. [CrossRef]
7. Bouzid, S.; Bouaouadja, N. Effect of Impact Angle on Glass Surfaces Eroded by Sand Blasting. *J. Eur. Ceram. Soc.* **2000**, *20*, 481–488. [CrossRef]
8. Zhou, J.; Ai, N.; Wang, L.; Zheng, H.; Luo, C.; Jiang, Z.; Yu, S.; Cao, Y.; Wang, J. Roughening the White OLED Substrate's Surface through Sandblasting to Improve the External Quantum Efficiency. *Org. Electron.* **2011**, *12*, 648–653. [CrossRef]
9. Su, N.; Yue, L.; Liao, Y.; Liu, W.; Zhang, H.; Li, X.; Wang, H.; Shen, J. The Effect of Various Sandblasting Conditions on Surface Changes of Dental Zirconia and Shear Bond Strength between Zirconia Core and Indirect Composite Resin. *J. Adv. Prosthodont.* **2015**, *7*, 214–223. [CrossRef]
10. Yetik, O.; Koçoğlu, H.; Yıldıran Avcu, Y.; Avcu, E.; Sınmazçelik, T. The Effects of Grit Size and Blasting Pressure on the Surface Properties of Grit Blasted Ti6Al4V Alloy. *Mater. Today Proc.* **2020**, *32*, 27–36. [CrossRef]
11. Wang, H.-Y.; Zhu, R.-F.; Lu, Y.-P.; Xiao, G.-Y.; He, K.; Yuan, Y.F.; Ma, X.-N.; Li, Y. Effect of Sandblasting Intensity on Microstructures and Properties of Pure Titanium Micro-Arc Oxidation Coatings in an Optimized Composite Technique. *Appl. Surf. Sci.* **2014**, *292*, 204–212. [CrossRef]
12. *ISO 25178-2:2021*; Geometrical Product Specifications (GPS)—Surface Texture: Areal—Part 2: Terms, Definitions, and Surface Texture Parameters. International Organization for Standardization: Geneva, Switzerland, 2021. Available online: https://www.iso.org/fr/standard/74591.html (accessed on 16 April 2023).
13. Valverde, G.B.; Jimbo, R.; Teixeira, H.S.; Bonfante, E.A.; Janal, M.N.; Coelho, P.G. Evaluation of Surface Roughness as a Function of Multiple Blasting Processing Variables. *Clin. Oral Implant. Res.* **2013**, *24*, 238–242. [CrossRef]
14. Bobrovskij, I.N. How to Select the Most Relevant Roughness Parameters of a Surface: Methodology Research Strategy. *IOP Conf. Ser. Mater. Sci. Eng.* **2018**, *302*, 012066. [CrossRef]
15. Ho, H.S.; Bigerelle, M.; Vincent, R.; Deltomb, R. Correlation Modeling between Process Condition of Sandblasting and Surface Texture: A Multi-scale Approach. *Scanning* **2016**, *38*, 191–201. [CrossRef]
16. Dong, W.P.; Sullivan, P.J.; Stout, K.J. Comprehensive Study of Parameters for Characterising Three-Dimensional Surface Topography: III: Parameters for Characterising Amplitude and Some Functional Properties. *Wear* **1994**, *178*, 29–43. [CrossRef]
17. Chetwynd, D.G. Slope Measurement in Surface Texture Analysis. *J. Mech. Eng. Sci.* **1978**, *20*, 115–119. [CrossRef]
18. Guo, Y.; Zhou, D.; Li, D.; Zhao, W.; Wang, Y.; Pang, L.; Shi, Z.; Zhou, T.; Sun, S.; Singh, C.; et al. Improved Energy Storage Performance of Sandwich-Structured P(VDF-HFP)-Based Nanocomposites by the Addition of Inorganic Nanoparticles. *J. Mater. Chem. C* **2023**, *11*, 6999–7009. [CrossRef]
19. Barros, H.D.O.; Abreu, R.F.; Abreu, T.O.; de Sousa, W.V.; Nogueira, F.E.A.; do Carmo, F.F.; de Morais, J.E.V.; do Nascimento, J.P.C.; da Silva, M.A.S.; da Silva, R.S.; et al. High Thermal Stability of the Microwave Dielectric Properties of $ZnNb_2O_6$ with $CaTiO_3$ Addition. *Phys. B Condens. Matter* **2024**, *695*, 416547. [CrossRef]
20. Persson, B.N.J. On the Fractal Dimension of Rough Surfaces. *Tribol. Lett.* **2014**, *54*, 99–106. [CrossRef]
21. Hutchings, I.M. A Model for the Erosion of Metals by Spherical Particles at Normal Incidence. *Wear* **1981**, *70*, 269–281. [CrossRef]
22. Gillström, P.; Jarl, M. Replacement of Pickling with Shot Blasting for Wire Rod Preparation. *Scand. J. Metall.* **2004**, *33*, 269–278. [CrossRef]
23. Ma, H.M.; Gao, X.-L.; Reddy, J. A Microstructure-Dependent Timoshenko Beam Model Based on a Modified Couple Stress Theory. *J. Mech. Phys. Solids* **2008**, *56*, 3379–3391. [CrossRef]
24. Chaudhri, M.M.; Walley, S.M. Damage to Glass Surfaces by the Impact of Small Glass and Steel Spheres. *Philos. Mag. A* **1978**, *37*, 153–165. [CrossRef]
25. Maeda, H.; Egami, N.; Kagaya, C.; Inoue, N.; Takesita, H.; Ito, K. Analysis of Particle Velocity and Temperature Distribution of Struck Surface in Fine Particle Peening. *Trans. Jpn. Soc. Mech. Eng.* **2001**, *67*, 2700–2706. [CrossRef]
26. Ciszak, C.; Popa, I.; Monceau, D.; Chevalier, S. High Temperature Behaviour of Ti Alloys in Moist Air. *Ann. Chim. Sci. Mater.* **2015**, *39*, 149–157. [CrossRef]
27. Melentiev, R.; Fang, F. Investigation of Erosion Temperature in Micro-Blasting. *Wear* **2019**, *420–421*, 123–132. [CrossRef]
28. Zahouani, H.; Vargiolu, R.; Loubet, J.-L. Fractal Models of Surface Topography and Contact Mechanics. *Math. Comput. Model.* **1998**, *28*, 517–534. [CrossRef]
29. Oshida, Y.; Munoz, C.A.; Winkler, M.M.; Hashem, A.; Itoh, M. Fractal Dimension Analysis of Aluminum Oxide Particle for Sandblasting Dental Use. *Bio Med. Mater. Eng.* **1993**, *3*, 117–126. [CrossRef]

30. Perrotti, V.; Aprile, G.; Degidi, M.; Piattelli, A.; Iezzi, G. Fractal Analysis: A Novel Method to Assess Roughness Organization of Implant Surface Topography. *Int. J. Periodontics Restor. Dent.* **2011**, *31*, 632.
31. Berkmans, F.; Lemesle, J.; Guibert, R.; Wieczorowski, M.; Brown, C.; Bigerelle, M. Two 3D Fractal-Based Approaches for Topographical Characterization: Richardson Patchwork versus Sdr. *Materials* **2024**, *17*, 2386. [CrossRef]
32. Kelechava, B. ASME B46.1-2019: Surface Texture (Roughness, Waviness, Lay). *The ANSI Blog*, 7 August 2020.
33. Krystek, M. A Fast Gauss Filtering Algorithm for Roughness Measurements. *Precis. Eng.* **1996**, *19*, 198–200. [CrossRef]
34. Yuan, Y.-B.; Qiang, X.-F.; Song, J.-F.; Vorburger, T.V. A Fast Algorithm for Determining the Gaussian Filtered Mean Line in Surface Metrology☆. *Precis. Eng.* **2000**, *24*, 62–69. [CrossRef]
35. Hara, S.; Tsukada, T.; Sasajima, K. An In-Line Digital Filtering Algorithm for Surface Roughness Profiles. *Precis. Eng.* **1998**, *22*, 190–195. [CrossRef]
36. Blunt, L.; Jiang, X. *Advanced Techniques for Assessment Surface Topography: Development of a Basis for 3D Surface Texture Standards "Surfstand"*; Elsevier: Amsterdam, The Netherlands, 2003.
37. Brinkmann, S. Development of a Robust Gaussian Regression Filter for Three-Dimensional Surface Analysis. In Proceedings of the 10th International Colloquium on Surface, Chemnitz, Germany, 31 January–2 February 2000.
38. *ISO 16610-21:2011*; Geometrical Product Specifications (GPS)—Filtration: Part 21: Linear Profiling Filters—Moving Average Filters. International Organization for Standardization: Geneva, Switzerland, 2011. Available online: https://www.iso.org/fr/standard/50176.html (accessed on 18 December 2024).
39. Raja, J.; Muralikrishnan, B.; Fu, S. Recent Advances in Separation of Roughness, Waviness and Form. *Precis. Eng.* **2002**, *26*, 222–235. [CrossRef]
40. Sahoo, P.; Barman, T.; Davim, J.P. Fractal Analysis in EDM. In *Fractal Analysis in Machining*; SpringerBriefs in Applied Sciences and Technology; Springer: Berlin/Heidelberg, Germany, 2011; Volume 3, pp. 69–81. ISBN 978-3-642-17921-1.
41. Chen, H.; Zhou, Y. Fractal Characteristics of 3D Surface Topography in Laser Machining. *IOP Conf. Ser. Mater. Sci. Eng.* **2018**, *382*, 042045. [CrossRef]
42. Brown, C.A.; Charles, P.D.; Johnsen, W.A.; Chesters, S. Fractal Analysis of Topographic Data by the Patchwork Method. *Wear* **1993**, *161*, 61–67. [CrossRef]
43. Mandelbrot, B. How Long Is the Coast of Britain? Statistical Self-Similarity and Fractional Dimension. *Science* **1967**, *156*, 636–638. [CrossRef]
44. Brown, C.A.; Hansen, H.N.; Jiang, X.J.; Blateyron, F.; Berglund, J.; Senin, N.; Bartkowiak, T.; Dixon, B.; Le Goïc, G.; Quinsat, Y.; et al. Multiscale Analyses and Characterizations of Surface Topographies. *CIRP Ann.* **2018**, *67*, 839–862. [CrossRef]
45. Efron, B.; Tibshirani, R. Bootstrap Methods for Standard Errors, Confidence Intervals, and Other Measures of Statistical Accuracy. *Stat. Sci.* **1986**, *1*, 54–75. [CrossRef]
46. Lieblich, M.; Barriuso, S.; Ibáñez, J.; Ruiz-de-Lara, L.; Díaz, M.; Ocaña, J.L.; Alberdi, A.; González-Carrasco, J.L. On the Fatigue Behavior of Medical Ti6Al4V Roughened by Grit Blasting and Abrasiveless Waterjet Peening. *J. Mech. Behav. Biomed. Mater.* **2016**, *63*, 390–398. [CrossRef]
47. Yang, J.; Song, Y.; Dong, K.; Han, E.-H. Research Progress on the Corrosion Behavior of Titanium Alloys. *Corros. Rev.* **2023**, *41*, 5–20. [CrossRef]
48. Yang, C.-K.; Cheng, C.-P.; Mai, C.-C.; Cheng Wang, A.; Hung, J.-C.; Yan, B.-H. Effect of Surface Roughness of Tool Electrode Materials in ECDM Performance. *Int. J. Mach. Tools Manuf.* **2010**, *50*, 1088–1096. [CrossRef]
49. Bok, W.-M.; Kim, S.-Y.; Lee, S.-J.; Shin, G.-S.; Park, J.-M.; Lee, M.-H. Surface Characteristics and Bioactivation of Sandblasted and Acid-Etched (SLA) Ti-10Nb-10Ta Alloy for Dental Implant. *Int. J. Precis. Eng. Manuf.* **2015**, *16*, 2185–2192. [CrossRef]
50. Bigerelle, M.; Giljean, S.; Anselme, K. Existence of a Typical Threshold in the Response of Human Mesenchymal Stem Cells to a Peak and Valley Topography. *Acta Biomater.* **2011**, *7*, 3302–3311. [CrossRef]